Highly Refractory Peridotites on Macquarie Island and the Case for Anciently Depleted Domains in the Earth's Mantle

ARJAN H. DIJKSTRA[1]*, DMITRY S. SERGEEV[1], CARL SPANDLER[2†], THOMAS PETTKE[2], THOMAS MEISEL[3] AND PETER A. CAWOOD[4]

[1]INSTITUT DE GEOLOGIE ET D'HYDROGEOLOGIE, UNIVERSITE DE NEUCHATEL, RUE EMILE ARGAND 11, CP 158, NEUCHATEL, CH-2009, SWITZERLAND

[2]INSTITUTE OF GEOLOGICAL SCIENCES, UNIVERSITY OF BERN, BALTZERSTRASSE 1+3, CH-3012 BERN, SWITZERLAND

[3]DEPARTMENT OF GENERAL AND ANALYTICAL CHEMISTRY, UNIVERSITY OF LEOBEN, LEOBEN 8700, AUSTRIA

[4]SCHOOL OF EARTH AND ENVIRONMENT, UNIVERSITY OF WESTERN AUSTRALIA, PERTH, WA 6009, AUSTRALIA

Macquarie Island (Southern Ocean) is a fragment of Miocene ocean crust and upper mantle formed at a slow-spreading ridge system, uplifted and currently exposed above sea-level. The crustal rocks on the island have unusually enriched compositions and the strong signature of an enriched source requires low overall degrees of melt depletion in the underlying mantle. Peridotites on the island, however, are highly refractory harzburgites that can be modeled as residues of >20–25% of near-fractional melting from which all the free clinopyroxene was melted out. The peridotites have some of the highest spinel Cr-numbers (0·40–0·49) and lowest orthopyroxene-core Al_2O_3 concentrations (2·7–3·0 wt %) reported so far for oceanic peridotites. The peridotites were subsequently modified by melt–rock reactions underneath the Miocene ridge system. The refractory character of the peridotites is inconsistent with the slow-spreading ridge setting as well as with the enriched character of the overlying crust, and must indicate a previous depletion event; the peridotites are not the source residue of the overlying ocean crust on Macquarie Island. Osmium isotopic compositions of peridotite samples are very unradiogenic ($^{187}Os/^{188}Os = 0·1194–0·1229$) compared with normal abyssal peridotites and indicate a long-lived rhenium depletion. Proterozoic rhenium-depletion ages indicate that these rocks have preserved a memory of an old mantle melting event. We argue that the Macquarie Island harzburgites are samples from an anciently depleted refractory mantle reservoir that may be globally important, but that is generally overlooked because of its sterility; that is, its inability to produce basalts. This reservoir may preserve key information about the history of the Earth's mantle as a whole.

KEY WORDS: *abyssal peridotite; ophiolite; petrology; Re–Os isotopes; trace elements; geochemistry*

INTRODUCTION AND GEOLOGICAL SETTING

Macquarie Island is a fragment of Miocene ocean crust underlain by upper mantle rocks that was uplifted and exposed above sea-level in an entirely intra-oceanic setting, without being obducted onto a continental margin (Varne *et al.*, 2000; Goscombe & Everard, 2001). Macquarie Island is considered by many as a type-locality of oceanic crust and upper mantle and as a key link between oceanic basement and ophiolites. Several workers have pointed out the similarity between the crustal section on the island, which consists of sediments, volcanic rocks, a sheeted dyke complex, and gabbros including layered gabbros (Fig. 1a), and the 'classical' ophiolite pseudo-stratigraphic sequence (Varne & Rubenach, 1972;

---

*Corresponding author. Telephone: +41 32 718 2581.
E-mail: arjan.dijkstra@unine.ch
†Present address: School of Earth and Environmental Sciences, James Cook University, Townsville, QLD 4811, Australia.
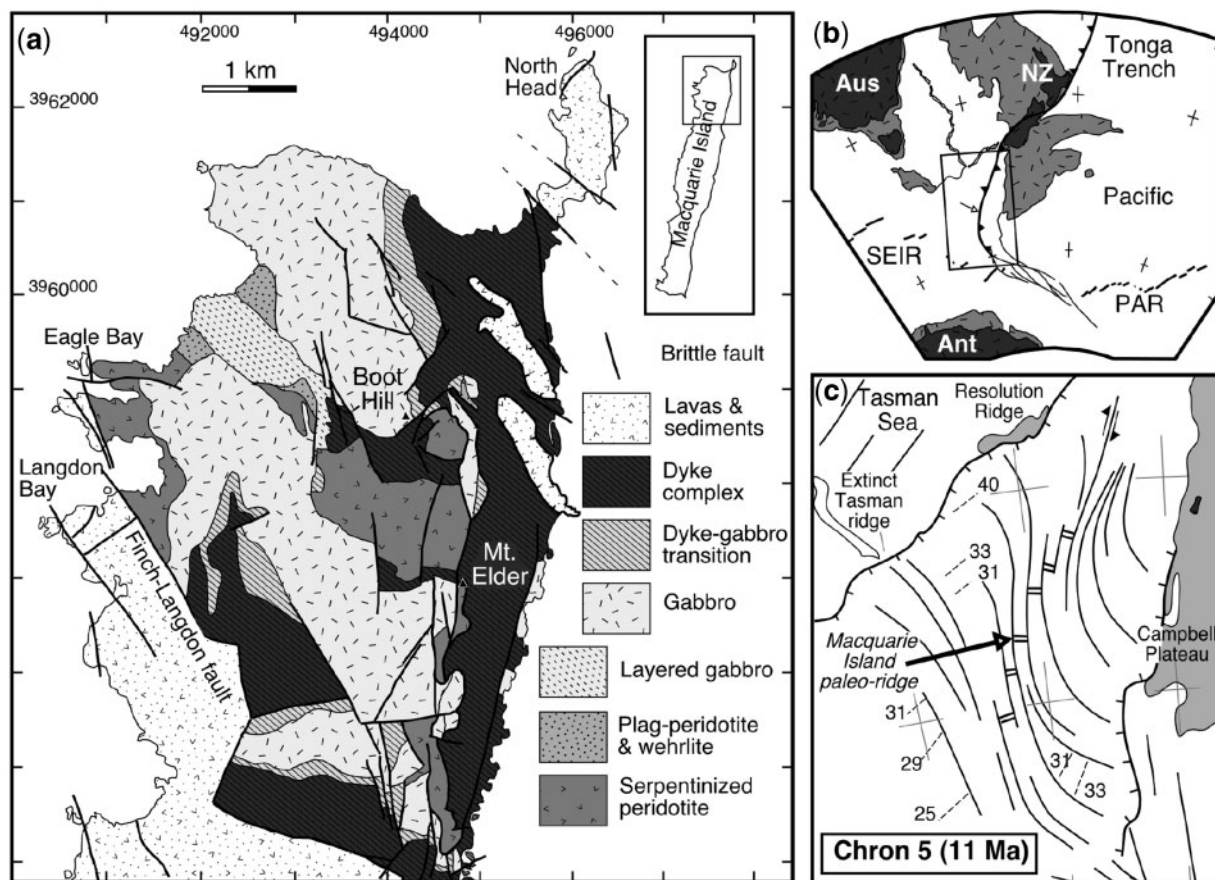
Fig. 1. (a) Map of the northern part of Macquarie Island, modified from Goscombe & Everard (2001). (b) Location of Macquarie Island (indicated by arrow) in relation to Australia (Aus), Antarctica (Ant), South East Indian Ridge (SEIR), Pacific–Antarctic Ridge (PAR), and Tonga–Kermadec Trench. (c) Plate reconstruction for 11 Ma (after Lamarche *et al.*, 1997), 2–3 Myr before the time of formation of the ocean crust exposed on Macquarie Island. Grid references are in UTM-WGS'84 coordinates.

Griffin & Varne, 1980; Christodoulou, 1994; Bazylev & Kamenetsky, 1998). It is also considered to be a key location to test the genetic link between ocean crust and residual oceanic mantle.

Recent work on the island has shown that the formation history of the island is complex. Field relations suggest that the volcanic rocks, dykes and gabbros on the island formed during a sequence of magmatic episodes, and there is no reason, *a priori*, to assume that the main pseudo-stratigraphic units are co-magmatic (Dijkstra & Cawood, 2004). Another unusual aspect is the general scarcity or lack of normal mid-ocean ridge basalt (N-MORB) igneous rocks on the island, with most volcanic rocks having enriched (E-)MORB affinities (Kamenetsky *et al.*, 2000; Kamenetsky & Maas, 2002; Varne *et al.*, 2003). Another issue is the unusually refractory character of the mantle rocks on the island, more depleted in fusible components than expected from the tectonic setting and reconstructed spreading rate of the Macquarie paleo-ridge system (Bazylev & Kamenetsky, 1998; Wertz, 2003;

Dijkstra & Cawood, 2004). It is the nature and origin of this strong mantle depletion in particular that we will address in detail in this paper. We show that the peridotites are among the most refractory samples of the oceanic mantle found so far in the modern oceans, and we use Os isotopes to argue that the mantle depletion is ancient, probably Proterozoic in age.

Macquarie Island is a fragment of the South Tasmanian Ocean Basin, a relatively small, wedge-shaped oceanic basin that formed by seafloor spreading between the eastern margin of the Campbell Plateau and the Tasman Sea from the Late Eocene onwards (Fig. 1b and c). Macquarie Island was uplifted when the divergent plate boundary became transpressional at about 5 Ma (Sutherland, 1995; Lamarche *et al.*, 1997). This led to the formation of the Hjort Trench–Macquarie Ridge–Puysegur Trench–Alpine Fault Zone system that now marks the Australian–Pacific plate boundary in the region (Fig. 1b). Plate reconstructions show that seafloor spreading was highly oblique (dextral) and slow to ultraslow, with a calculated full

spreading rate of *c.* 2 cm/year, between 11 and 5 Ma (Sutherland, 1995; Lamarche *et al.*, 1997).

COMPOSITION AND AGE OF THE OCEANIC CRUSTAL ROCKS

Kamenetsky and co-workers (Kamenetsky *et al.*, 2000; Kamenetsky & Maas, 2002) found that compositions of fresh volcanic glasses from lava localities around the island ranged from transitional to highly enriched mid-ocean ridge basalts (T- to E-MORB), to silica-undersaturated basalts. The compositional variation of the glasses is well expressed by the La/Sm ratio, as this ratio is relatively insensitive to fractionation (White & Schilling, 1978; Hofmann, 1997). $(La/Sm)_n$ in primitive Macquarie Island glasses ranges from 0·9 to 4·9, with the highest values being associated with E-MORB and silica-undersaturated basalts [throughout the text, the subscript n refers to data normalized to the Primitive Mantle estimate of McDonough & Sun (1995)]. Moreover, Kamenetsky and co-workers found systematic relations between La/Sm ratios and Nd, Sr, and Pb isotope ratios: Pb isotope ratios in the most enriched glasses (i.e. those with the highest La/Sm) tend towards those of HIMU-type basalts (high-μ: high $^{238}U/^{204}Pb$). HIMU signatures are generally thought to be derived from a mantle source containing recycled oceanic crustal material (e.g. Hofmann, 1997).

Varne and co-workers (Varne & Rubenach, 1972; Varne *et al.*, 2000) noted that dolerites on the island resemble MORB in general, but that, based on trace elements, 'true' N-MORB compositions are absent. In comparison, the plutonic rocks on the island have more variable major element and mineralogical compositions, ranging from ultramafic cumulates such as plagioclase-wehrlites, to troc-tolites, olivine-gabbros, oxide gabbros, and highly differen-tiated gabbros (Christodoulou, 1994). Major element compositions and phenocryst assemblages in the volcanic rocks and dykes resemble those of the gabbros, suggesting that all the igneous rocks on the island are related (Griffin & Varne, 1980; Christodoulou, 1994; Varne *et al.*, 2000).

Recent biostratigraphic ages obtained from sediments intercalated with pillow lavas were 9·5–9·3 Ma for the northern part of the island and 9·01–8·78 Ma for the south-ern part (Quilty *et al.*, 2008). Precise U–Pb SHRIMP zircon dating gave crystallization ages for three gabbros from the northern part of the island between 9·0 and 8·6 Ma (A. H. Dijkstra & P. A. Cawood, unpublished data). Full description and scientific discussion of these results will be presented elsewhere.

ANALYTICAL METHODS

Samples of mantle rocks were studied using conventional light microscopy and scanning electron microscopy (SEM). Minerals were analyzed for major elements using A JEOL JXA-8200 Superprobe at 15 kV and 20 nA, using spot sizes between 2 and 10 μm, at the University of Bern. Counting times were typically 20 s for Si, Mg, Fe, Ca, Na and Al, and 30 s for Ti, Cr, Ni and Mg. Well-characterized natural and synthetic minerals (silicates and oxides) were used for standardization.

Trace element concentrations of clinopyroxene crystals in ∼80–100 μm 'thick sections' of peridotites, and in clino-pyroxene mineral separates mounted in epoxy disks, were analyzed by laser-ablation inductively coupled plasma mass spectrometry (LA-ICP-MS) at the University of Bern, employing a 193 nm ArF Excimer laser and an ELAN DRC-e quadrupole ICP-MS system, at conditions similar to those reported by Pettke (2008). SRM 612 glass from NIST was used as the external standard and Ca was used as the internal standard. Data reduction was done using LAMTRACE (Jackson, 2008). Backgrounds (blanks) were typically counted for 60 s before ablation and standard glasses were ablated and counted for 40–60 s with a 60 μm spot size. Detection limits were determined for each analysis and were typically 1–3 ppb for Y, Nb, Cs, La, Ce, Pr, Eu, Sm, Tb, Ho, Tm, Lu, Th and U; 4–6 ppb for Rb, Sr, Zr, Nd, Sm, Gd, Dy, Er, Hf and Pb; 7–12 ppb for Ba, Yb and V; 40 ppb for Sc; 0·2 ppm for Ni; and 0·5 ppm for Cr at the commonly used crater size of 90 μm. External precision of the elemental concentrations determined from repeated SRM 612 standard analysis was 2·7% for Ni, 1–2% for La, Sm, Er, Ho, Yb, Pb and Cr, and <1% for all other elements. Analytical precision is lower in cases of low count rates as a result of increased counting statistics uncertainty, as measured clinopyroxene trace element concentrations were typically 1–4 orders of magnitude lower than in the SRM 612 glass. Relatively large spot sizes of 90–120 μm and long ablation or counting times of 60–90 s were employed for the analyses of the unknowns because of the very trace-element-depleted nature of the pyroxene in the studied samples. Because of the small sizes of the pyroxene, this resulted almost invari-ably in some overlap of the beam on cracks during part of the analyses. Counts of Pb, Cs, Ba and Rb were monitored during analysis and high counts were seen to be associated with cracks. Parts of the time signal with high counts of these elements were eliminated from the subsequent con-centration calculations. This resulted in effective counting time signals of 10–90 s. Possible mass-load dependent matrix effect variations between standards and unknowns as a result of different spot sizes are almost certainly insig-nificant compared with uncertainties of the standard glass for the set-up and optimization conditions employed in our study (Pettke, 2008).

Clinopyroxene was extracted from five peridotite samples and from a centimeter-scale gabbroic vein within the mantle rocks by means of conventional heavy liquid and magnetic methods. Macroscopically visible vein material was removed from the peridotite samples prior to crushing, but (diffuse) microveins ($<300\,\mu m$) observed in thin sections were almost certainly present in the crushed material. In the case of two samples, two clinopyroxene fractions obtained by magnetic (Frantz) separation were prepared. The separates were purified by hand-picking of optically transparent, inclusion-free crystals and analyzed for Sr and Sm–Nd isotopes at the University of Melbourne, following the methods and protocols of Maas *et al.* (2005). Aliquots (30–100 mg) of acid-washed (2M HCl) mineral separates were dissolved on a hotplate (in HF–HNO$_3$ and HCl) and spiked with mixed ^{149}Sm–^{150}Nd tracer. Sm, Nd and Sr were extracted using EICHROM^{TM} RE, LN and Sr-resins. Total blanks are ≤ 10 pg for Nd and ≤ 30 pg for Sr. Isotopic data were obtained on a NU Instruments MC-ICP-MS system coupled to a CETAC Aridus desolvating nebulizer. Mass bias was corrected by normalizing to ^{146}Nd/^{145}Nd $= 2\cdot0719425$ (equivalent to ^{146}Nd/^{144}Nd $= 0\cdot7219$) and ^{86}Sr/^{88}Sr $= 0\cdot1194$, using the exponential law; Kr interference Sr 'memory effects' were removed following Waight *et al.* (2002). Spike subtraction for Nd and Sm was carried out on-line. Data are reported relative to La Jolla Nd $= 0\cdot511860$ and SRM 987 $= 0\cdot710230$. Results for international standards (BCR-1, $0\cdot70502 \pm 5$, $0\cdot512641 \pm 18$; BHVO-1, $0\cdot70348 \pm 4$, $0\cdot512998 \pm 18$; JNdi-1 $0\cdot512113 \pm 22$; E&A carbonate $0\cdot70801 \pm 5$; EN-1 modern seawater $0\cdot70916 \pm 3$, all errors 2 SD) compare well with those obtained by thermal ionization mass spectrometry (TIMS). Typical in-run precisions (2 SE) are $\pm 0\cdot000010$ (or $0\cdot004\%$, Nd) and $\pm 0\cdot000022$ (Sr), but reached $\pm 0\cdot012\%$ for several of the smaller (<10 ng Nd) samples studied here. However, standard runs at similar signals confirm that such runs still yield accurate results. ^{147}Sm/^{144}Nd is $0\cdot1380 \pm 2$ (2 SD, BCR-1) and $0\cdot1493 \pm 3$ (BHVO-1); the ^{147}Sm decay constant is $6\cdot54 \times 10^{-12}$ year^{-1}; present-day ^{147}Sm/^{144}Nd$_{CHUR} = 0\cdot1967$ and ^{143}Nd/^{144}Nd$_{CHUR} = 0\cdot512638$.

Aliquots of 20–30 mg of hand-picked clinopyroxene from the same sample volume were also analyzed for trace element concentration using solution ICP-MS at the University of Melbourne. These 'bulk clinopyroxene' batches were washed with distilled 0·5M HCl prior to dissolution in closed Savillex beakers using HF–HNO$_3$ and HNO$_3$. Dried nitrates were re-dissolved with multi-isotopic spike solution to correct for drift during ICP-MS analysis (see Eggins *et al.*, 1997). Samples were analyzed on a Varian quadrupole ICP-MS system, using four dilutions of the same BHVO-1 sample as calibration standards.

Highly siderophile element concentrations (HSE: Os, Ir, Ru, Pd, Pt, Re) were determined in whole-rock samples of peridotites. Peridotites were crushed and agate-milled using a protocol tuned to eliminate metal contamination. ^{187}Os/^{188}Os isotope ratios and HSE concentrations in peridotites and in one gabbroic vein were determined using the method of isotope dilution described by Meisel *et al.* (2003) on a quadrupole ICP-MS system (HP 7500, Agilent Technologies) at the University of Leoben, Austria. Two grams of fine powdered samples, with the addition of a ^{99}Ru, ^{108}Pd, ^{185}Re, ^{190}Os, ^{191}Ir, ^{198}Pt mixed spike, were dissolved in a mixture of 5 ml HNO$_3$ and 2 ml HCl in closed quartz vials in a High Pressure Asher (HPA) system (Anton Paar–Perkin-Elmer Instruments, Graz) at 300°C and at a pressure of 125 bar for 4 h. In one digestion run, five samples, one reference material sample (i.e. TDB-1 Diabase Rock PGE Material, Natural Resources Canada, and OKUM Komatiite, Geolabs, Ontario, Canada) and one blank were dissolved. The Os isotope ratio and concentration were measured as volatile OsO$_4$ complex, which was directly fed into the ICP-MS system. The residue was centrifuged and dried down on a hot plate, and re-dissolved in 1·5 ml 0·1 mol/l HCl. The solution was filtered and introduced into a cation-exchange resin column (Dowex AG50Wx8 200–400 mesh, Fluka) connected directly to the tubing system of the peristaltic pump on the mass spectrometer. The time signal was monitored and the relevant, overlap-free part of the signal was used to calculate concentrations. Measurement errors of the average of seven independent concentration measurement of TDB-1 were found to be less 15% of the certified values (Pt 5·8 ppb and Pd 22·4 ppb). Concentrations of Os, Ir and Ru are not certified but compare very well with published ID-MS data. Too few data exist for OKUM to compare with our dataset. As the HSE concentrations in our samples are generally in the 1–10 ppb range, the combined uncertainty for measurement for all HSE in this range is estimated to be less than 15% relative.

The Macquarie samples were analyzed together with a series of mantle rocks from the Pindos Ophiolite (Greece). Two samples from Pindos were subsequently also digested and analyzed by conventional N-TIMS methods for Os isotopes at the Centre of Isotope Research in St. Petersburg, Russia, and ^{187}Os/^{188}Os ratios were found to be identical within 0·5%.

RESULTS
Textures and mineral compositions in mantle rocks

The peridotite samples studied originate from an area immediately east of Boot Hill (Fig. 1a; see also Table A1 in the supplementary dataset, available for downloading at

Table 1: Representative spinel analyses determined by electron microprobe

	M2-1	M3-2	M3-3	M11-1	M11-3	M11-4	M21-2
SiO_2	0·01	0·02	0·00	0·04	0·03	0·04	0·04
FeO*	16·80	17·76	17·92	18·4	17·77	20·02	16·37
CaO	—	0·02	0·02	0·01	0·02	—	—
Na_2O	—	0·02	0·06	—	0·06	0·02	0·01
MgO	15·14	14·21	14·44	13·8	14·27	14·16	15·23
Cr_2O_3	35·61	36·65	36·09	39·97	41·94	39·06	37·18
TiO_2	0·02	0·04	0·00	0·08	0·02	0·10	0·05
Al_2O_3	32·11	30·18	32·20	27·54	26·71	26·45	31·57
NiO	0·12	0·14	0·19	0·10	0·15	0·13	0·16
Total	99·81	99·04	100·9	99·94	100·9	99·99	100·6
FeO[1]	13·86	14·72	15·20	15·30	14·66	14·61	13·86
Fe_2O_3	3·27	3·38	3·03	3·45	3·45	6·01	2·79
Cr-no.	0·43	0·45	0·43	0·49	0·51	0·50	0·44
Mg-no.	0·66	0·63	0·63	0·62	0·63	0·63	0·66

*Total Fe given as FeO.
[1]Fe^{2+}/Fe^{3+} distribution calculated assuming charge balance and spinel stoichiometry.

http://www.petrology.oxfordjournals.org/), a block of peridotites entirely enclosed within gabbros and dyke complex rocks. The Boot Hill area is one of the few areas on the central plateau that has outcrops of mantle rocks. In addition, one sample (M2l-2) was studied from Eagle Bay (Fig. la), from outcrops of mantle rocks structurally a few hundred meters below a zone of plagioclase-dunites, wehrlites and layered troctolite gabbros, which can be best described as a crust–mantle transition zone. Peridotites in both areas are cross-cut by abundant millimeter- to meter-scale gabbroic veins and dykes. Thin sections of representative samples were analyzed by microscope, SEM and electron microprobe. Representative spinel, orthopyroxene and clinopyroxene compositions are given in Tables 1–3.

Although we sampled the freshest peridotites available, we found that the samples are all strongly to moderately serpentinized (l0–60% primary or magmatic phases remain). Secondary alteration phases are serpentine, 'bastite', magnetite, talc, rare secondary amphibole, and in a few cases, carbonates in thin veins (Table Al). In one peridotite sample (Mll-l), we found a thin, discontinuous vein of clinopyroxene together with relics of plagioclase, mostly altered to a fine-grained isotropic mineral aggregate. Apart from such veins, the peridotites are essentially spinel-harzburgites: no interstitial plagioclase or alteration products of plagioclase, such as found in typical plagioclase-peridotites (e.g. Dijkstra *et al.*, 200l), were observed. Microstructures are coarse porphyroclastic; olivine grains are typically >l mm and contain well-defined, widely spaced kinkband-type subgrain boundaries (Fig. 2a).

A striking feature of all these samples is the low modal abundance (<2 vol. %) and small grain size (typically <300 µm) of clinopyroxene. Different textural types of clinopyroxene were recognized: clinopyroxene is present as exsolutions in orthopyroxene, as grains along kinkbands in orthopyroxene, as grains or seams on orthopyroxene grain boundaries, as part of typically 500 µm-sized spinel–clinopyroxene intergrowths resembling symplectites at orthopyroxene grain boundaries or within the olivine matrix, as part of thin microveins (±rare plagioclase), but rarely as interstitial grains within the olivine matrix (Fig. 2b–f). Primary clinopyroxene clasts were never observed.

Sample average Cr-numbers [i.e. molar $Cr/(Cr+Al)$ ratios] in spinel range from 0·40 to 0·49 (Fig. 3a). There is typically a positive correlation between Cr-number and TiO_2 concentrations in spinel within and between samples (Fig. 3b), with TiO_2-poor (<0·05 wt %) spinel generally having a Cr-number between 0·39 and 0·45, and the highest Cr-number (up to 0·52) in spinel containing up to 0·12 wt % TiO_2.

Al_2O_3 concentrations in the cores of orthopyroxene crystals are very low, typically 2·7–3·0 wt % (Fig. 4, Table 2), and decrease towards the rims (<2·4 wt %). The decrease in Al_2O_3 from core to rim is correlated with a decrease in Cr_2O_3 in orthopyroxene from l·0 to <0·5 wt %.

In general, there is no obvious, well-defined relation between the textural type of clinopyroxene within peridotite and major or minor element composition (Table 3). Typically, exsolved clinopyroxene is slightly richer in CaO

Table 2: Representative orthopyroxene analyses determined by electron microprobe

	M2-1 core	M2-1 rim	M3-2 core	M3-2 rim	M3-3 core	M3-3 rim	M11-1 core	M11-1 rim
SiO_2	55·13	56·02	56·07	56·11	56·07	56·56	56·75	57·26
FeO*	5·31	5·87	5·68	5·76	5·52	5·68	5·35	5·42
CaO	2·27	0·82	1·90	1·71	1·19	0·87	2·15	0·77
Na_2O	0·02	—	—	0·01	—	0·02	0·03	—
K_2O	n.d.	n.d.	n.d.	n.d.	0·06	0·05	0·01	—
MgO	32·48	34·25	33·45	33·59	33·46	34·00	33·23	34·24
Cr_2O_3	0·78	0·45	0·80	0·65	0·80	0·59	0·84	0·60
TiO_2	—	—	—	—	—	—	0·01	0·02
Al_2O_3	2·90	2·24	2·67	2·42	2·76	2·24	2·27	1·77
MnO	0·11	0·16	0·13	0·14	0·13	0·16	n.d.	n.d.
NiO	0·09	0·08	0·19	0·13	0·16	0·24	0·10	0·10
Total	99·09	99·90	100·9	100·5	100·2	100·4	100·7	100·2

	M11-3 core	M11-3 rim	M11-4 core	M21-2 core	M21-2 rim
SiO_2	56·32	56·31	56·30	55·28	55·76
FeO*	5·12	5·59	5·71	5·64	6·27
CaO	3·04	1·28	0·99	2·65	0·99
Na_2O	0·03	0·02	0·01	0·01	—
K_2O	—	—	—	0·01	0·01
MgO	32·64	33·33	33·73	31·84	33·49
Cr_2O_3	0·77	0·67	0·77	0·90	0·55
TiO_2	—	0·01	—	0·02	—
Al_2O_3	2·36	2·21	2·48	2·95	2·42
MnO	n.d.	n.d.	n.d.	n.d.	n.d.
NiO	0·11	0·11	0·11	0·10	0·06
Total	100·4	99·52	100·1	99·39	99·55

*Total Fe given as FeO.

($>$24 wt % CaO) than other textural types. In M3-2, clinopyroxene within a diffuse microvein is slightly richer in TiO_2 (0·03 wt %) than other types of clinopyroxene in the same sample, but in sample M11-1, which contains a microvein, all types of clinopyroxene have elevated TiO_2 ($>$0·07 wt %). Clinopyroxene grains from the centimeter-wide gabbroic vein in M11-5 are distinct: they have low CaO ($<$23 wt % in cores) and elevated TiO_2 ($>$0·4 wt %). Decrease in Al correlates with decrease in Cr in clinopyroxene. Typically, clinopyroxene exsolutions from orthopyroxene or clinopyroxene grains enclosed within orthopyroxene clasts have the highest Al_2O_3 and Cr_2O_3 concentrations, whereas clinopyroxene intergrown with spinel and interstitial clinopyroxene typically have lower concentrations of Al_2O_3 and Cr_2O_3.

Clinopyroxene trace element data for mantle rocks

Trace element concentrations in clinopyroxene were analyzed *in situ* in ∼80–100 μm 'thick sections', as well as in polished epoxy grain mounts of mineral separates (separated from 1–2 kg of rock) by LA-ICP-MS (see Table A2, supplementary dataset, for all analytical results). Trace element concentrations in clinopyroxene are generally low, well below those of primitive mantle (Figs 5 and 6). Yb_n is typically 0·55–0·75. The trace elements, in particular the middle rare earth elements (MREE), are highly variable within samples, a feature that is seen in each of the samples studied. REE patterns are generally U-shaped, with MREE depletions with respect to light REE (LREE) and heavy REE (HREE). In some grains Sm, Eu, and Nd

Table 3: Representative clinopyroxene analyses determined by electron microprobe

Text. type:[1]	M2-1 exsol	M2-1 in opx	M2-1 opx gb	M2-1 w. sp	M2-1 interst	M3-2 in opx	M3-2 gb selv	M3-2 w. sp	M3-2 interst	M3-2 diff. μvein
SiO_2	52·91	52·67	52·70	52·87	52·35	53·18	53·36	52·83	53·14	53·24
FeO^*	2·18	2·36	2·20	2·38	2·22	2·18	2·32	2·17	2·16	2·37
CaO	24·13	23·17	23·70	23·26	23·32	23·72	23·47	23·35	23·39	23·39
Na_2O	0·10	0·08	0·09	0·08	0·09	0·11	0·11	0·10	0·05	0·11
K_2O	—	—	0·05	0·01	—	—	0·01	0·01	—	—
MgO	16·44	17·21	17·24	17·06	17·10	16·97	17·28	17·29	16·99	17·13
Cr_2O_3	1·02	1·10	0·67	0·96	1·11	1·02	0·77	0·98	0·84	0·87
TiO_2	0·02	—	0·01	0·01	0·01	0·01	0·02	0·02	0·01	0·03
Al_2O_3	2·79	3·22	2·56	2·98	3·08	2·88	2·38	2·54	2·44	2·57
MnO	0·08	0·12	0·07	0·14	0·09	0·09	0·15	0·12	0·18	0·12
NiO	0·04	0·10	0·07	0·03	0·06	n.d.	0·03	0·04	0·03	0·04
Total	99·71	100·0	99·33	99·78	99·44	100·1	99·89	99·44	99·23	99·86

Text. type:[1]	M3-3 exsol	M3-3 in opx	M3-3 opx gb	M3-3 w. sp	M3-3 interst	M11-1 exsol	M11-1 opx gb	M11-1 μvein	M11-3 opx gb	M11-3 w. sp
SiO_2	52·91	52·67	53·28	52·79	52·68	53·69	52·67	52·68	53·24	53·67
FeO^*	1·98	2·24	2·28	1·89	2·15	1·98	2·40	2·26	2·31	2·12
CaO	24·43	23·90	23·48	24·05	23·65	24·27	23·19	23·74	23·11	23·66
Na_2O	0·04	0·06	0·06	0·05	0·06	0·14	0·13	0·15	0·22	0·17
K_2O	0·06	0·05	0·05	0·05	0·06	0·01	—	—	0·01	0·01
MgO	17·60	16·92	17·25	17·22	17·37	17·07	17·27	16·98	17·25	16·92
Cr_2O_3	0·63	1·10	0·94	0·75	0·93	1·19	1·10	1·16	1·14	0·91
TiO_2	—	—	—	0·01	—	0·09	0·08	0·08	0·02	—
Al_2O_3	2·10	3·18	2·91	2·42	2·81	2·44	2·78	2·83	2·86	2·21
MnO	0·07	0·05	0·05	0·08	0·03	n.d.	n.d.	n.d.	n.d.	n.d.
NiO	0·19	0·09	0·06	0·14	0·21	0·05	0·06	0·06	0·05	0·05
Total	100·0	100·3	100·4	99·45	99·94	101·0	99·73	100·0	100·3	99·79

Text. type:[1]	M11-4 exsol	M11-4 w. sp	M11-4 interst	M21-2 exsol	M21-2 opx gb	M21-2 w. sp	M21-2 vein cpx c	M11-5 gabb. vein	M11-5 gabb. vein	M11-5 g. vein cpx r
SiO_2	52·90	53·03	53·43	52·37	52·31	52·40	51·70	52·69	51·87	52·70
FeO^*	2·29	2·24	2·26	2·26	2·22	2·47	2·51	2·70	2·60	2·42
CaO	23·59	23·79	23·61	24·06	24·19	23·76	22·93	22·43	22·96	23·04
Na_2O	0·11	0·13	0·10	0·05	0·04	0·04	0·05	0·34	0·36	0·28
K_2O	—	0·01	0·01	—	—	—	—	—	—	—
MgO	17·07	16·83	17·65	16·87	17·09	17·42	16·86	16·67	16·25	16·89
Cr_2O_3	1·15	1·08	1·04	1·31	0·82	1·04	1·54	1·06	1·26	0·95
TiO_2	0·04	0·04	0·07	0·03	0·03	0·03	0·03	0·41	0·44	0·34
Al_2O_3	2·97	2·77	2·49	3·30	2·46	2·80	4·00	2·95	4·02	2·64
MnO	n.d.	n.d.	n.d.	n.d.	n.d.	n.d.	n.d.	0·18	0·11	0·10
NiO	0·04	0·05	0·06	0·02	0·06	0·03	0·05	0·05	—	0·03
Total	100·2	100·0	100·8	100·3	99·23	100·0	99·69	99·48	99·87	99·39

[1]Textural types of cpx: exsol, exsolved cpx in opx clast; in opx, cpx grain enclosed within opx clast; opx gb, cpx grain on opx grain boundary; w. sp, cpx within cpx–spinel intergrowth; interst, interstitial cpx grain within olivine matrix; gb selv., selvage-type rim of cpx on opx clast; diff. μvein, cpx as part of diffuse micro-vein; μvein, cpx as part of distinct, <300 μm wide vein; vein cpx c, core of cpx in >500 μm wide vein; gabb. vein, cpx within gabbroic vein (with plagioclase); g. vein cpx r, rim of cpx within gabbroic vein.
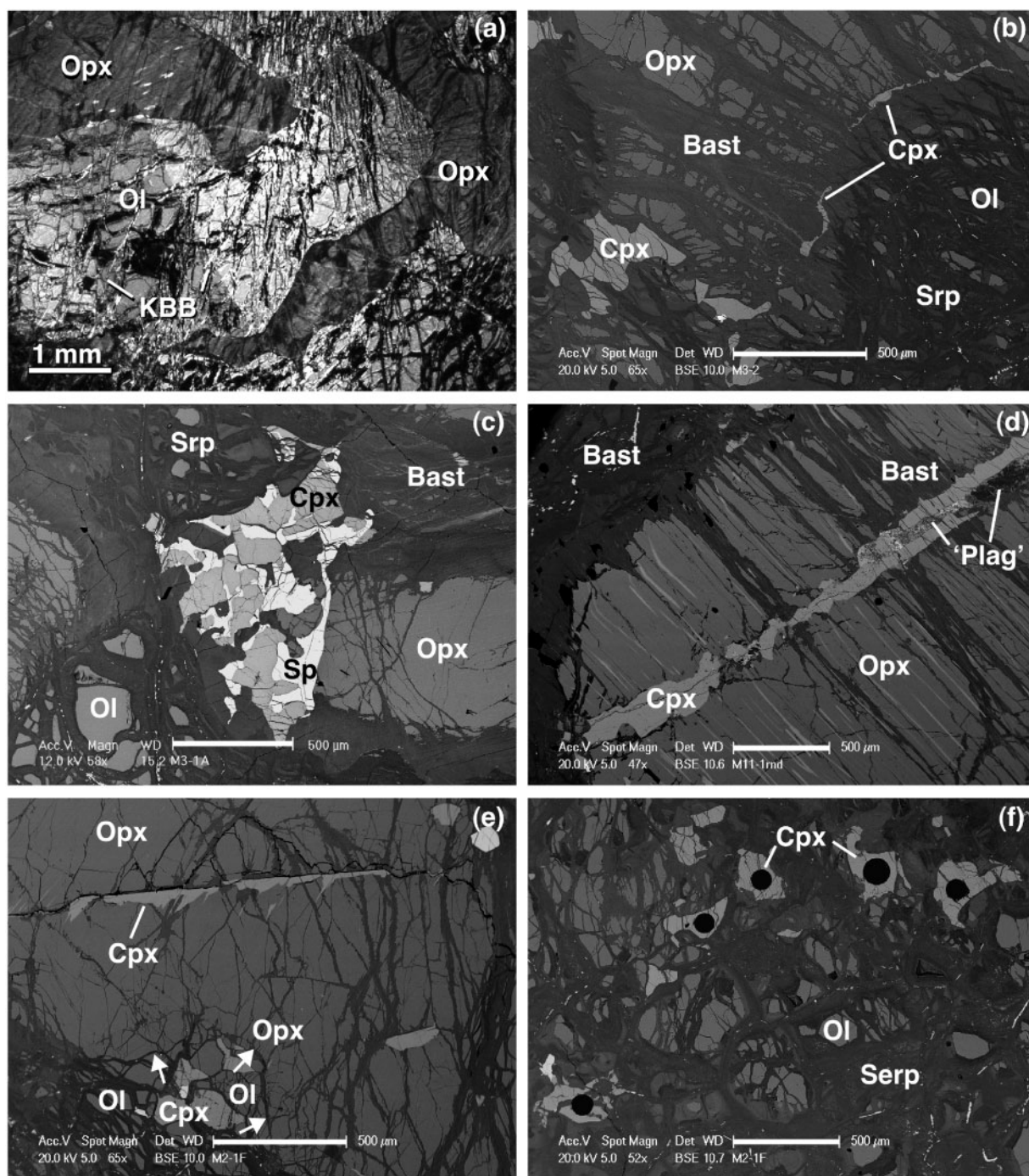*Total Fe given as FeO.

Fig. 2. Photomicrographs showing representative textures and clinopyroxene textural types in Macquarie Island peridotites. (a) Optical photomicrograph (crossed polars) showing corroded orthopyroxene clast surrounded by large olivines with well-defined kinkband boundaries ('KBB'). (b) Backscattered electron (BSE) SEM image showing clinopyroxene 'selvage' on orthopyroxene clast. (c) BSE SEM image showing spinel–clinopyroxene symplectite-like intergrowth. (d) BSE SEM image showing clinopyroxene microvein with some (now mostly altered) plagioclase cutting across an orthopyroxene clast containing thin clinopyroxene exsolution lamellae. (e) BSE SEM image showing a kinkband boundary in an orthopyroxene clast decorated with clinopyroxene in textural continuity with clinopyroxene exsolution lamellae; also shown is an embayment (indicated by white arrows) of olivine, clinopyroxene and spinel in the orthopyroxene clast. (f) BSE SEM image showing alignment of interstitial clinopyroxene grains within olivine matrix ('diffuse microvein'); dark circles are 90 and 120 μm laser-ablation spots. The scale bars in the SEM images (b)–(f) represent a length of 500 μm.
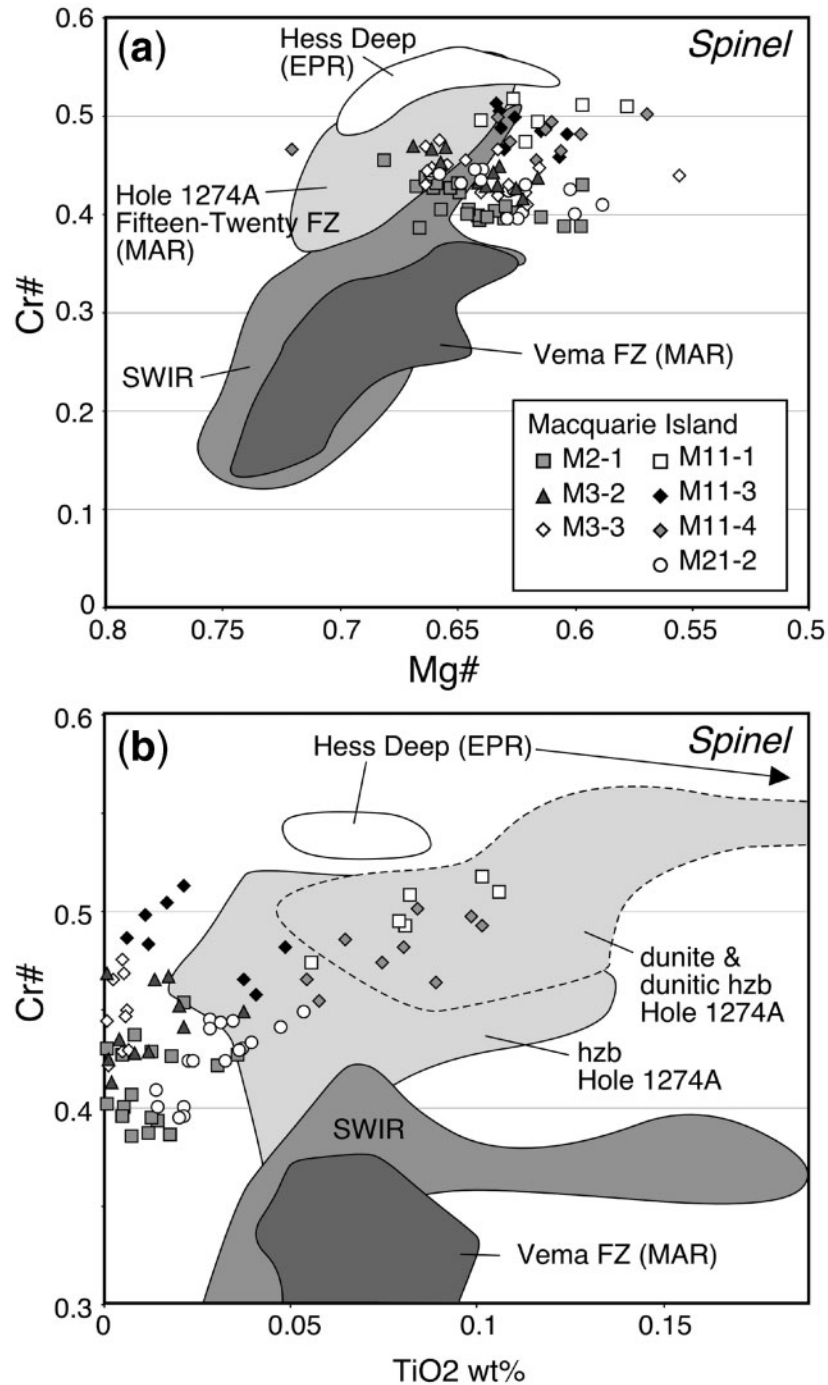
Fig. 3. Spinel compositions in Macquarie Island peridotites. (a) Cr-number [i.e. molar $Cr/(Cr+Al)$] vs Mg-number [i.e. molar $Mg/(Mg+Fe^{2+})$]. (b) Cr-number vs TiO_2 wt %. Fields for Vema Fracture Zone (Mid-Atlantic) spinel from Brunelli *et al.* (2006), for Southwest Indian Ridge (SWIR) from Seyler *et al.* (2003), for ODP Hole 1274 (Mid-Atlantic) from Seyler *et al.* (2007) and Suhr *et al.* (2008), and for Hess Deep (East Pacific Rise) from Dick & Natland (1996).

concentrations were lower than the analytical detection limits. The depth of the MREE 'trough' varies significantly amongst clinopyroxene grains separated from the same sample, with some clinopyroxene having nearly flat LREE–MREE patterns. Flat patterns, as found in clinopyroxene separates, were not found in thick sections. However, rare interstitial clinopyroxene grains, in particular those forming trails within the olivine matrix ('diffuse
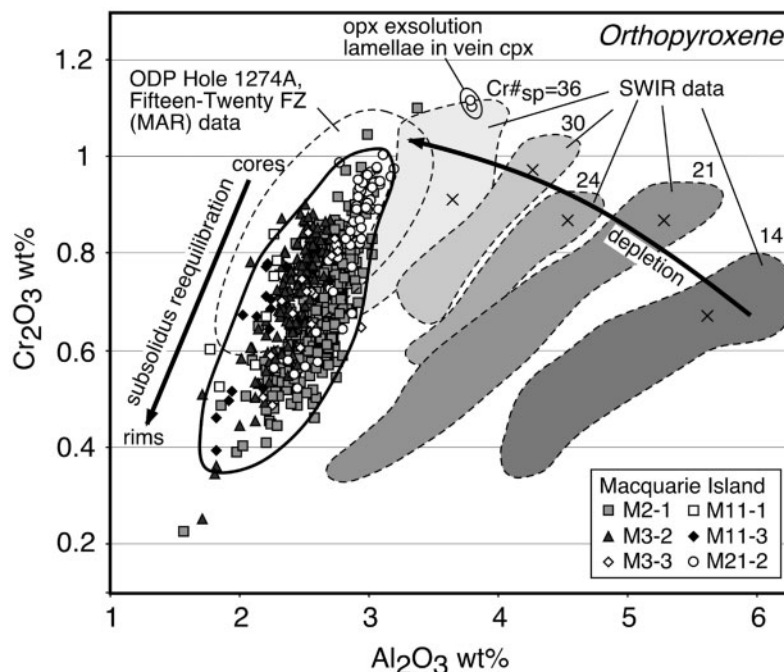
Fig. 4. Cr_2O_3 vs Al_2O_3 wt % for orthopyroxene in Macquarie Island peridotites. Fields for orthopyroxene in various peridotite samples from the Southwest Indian Ridge (SWIR) from the study of Seyler *et al.* (2003); crosses indicate typical orthopyroxene core compositions; numbers next to field indicate average Cr-number for coexisting spinel. Data for orthopyroxene from ODP Hole 1274A, Fifteen–Twenty Fracture Zone, Mid-Atlantic Ridge (MAR) from Seyler *et al.* (2007) and Suhr *et al.* (2008) are also shown for comparison. Bold subvertical arrow indicates trend of subsolidus re-equilibration (after Witt-Eickschen & Seck, 1991), whereas subhorizontal arrow indicates depletion trend.

microveins'), tend to have flatter LREE–MREE patterns than the other types of clinopyroxene, suggesting a general textural control on the trace element patterns. The most flat-patterned clinopyroxene generally still has concentrations of MREE–HREE well below those of the pyroxene from the centimeter-wide gabbroic vein. Only in the case of sample M21-2, three separated clinopyroxene grains were found that have similar, 'magmatic' clinopyroxene trace element patterns, with MREE–HREE$_n$ of 3–5. All clinopyroxene analyses show a gradual increase of normalized concentrations from Rb and Ba towards La and Nb (Fig. 6). $(Th/Nb)_n$ ratios are low (typically 0·1–0·6). Clinopyroxene generally displays negative Sr anomalies (Fig. 6), which are most pronounced in the samples that have weakly U-shaped to flat REE patterns, and that are also present in the gabbroic vein of sample M11-5.

The general shapes of the trace element patterns, including the negative Sr anomalies, were well reproduced by analysis of 20–30 mg bulk clinopyroxene grain batches by solution-ICP-MS (Fig. 6a, Table A3; also shown by dark grey lines in Figs 5a,b,c,e and 6b,c,e). These bulk analyses were most similar to the trace element analyses of single grains with relatively high MREE concentrations; that is, with relatively weakly U-shaped to flat patterns. These bulk analyses are, as expected, close to the calculated mean of the single grain analyses in each sample.

Sr and Sm–Nd isotope results for mantle clinopyroxene

Neodymium and Sr isotope data for clinopyroxene separates from five peridotite samples and from a 1 cm gabbroic vein (M11-5) are given in Table 4 and plotted in Fig. 7. The $^{143}Nd/^{144}Nd$ isotope ratios of the peridotite samples overlap within analytical uncertainty. The peridotite data are also identical to the data for the gabbroic vein within error. $^{147}Sm/^{144}Nd$ ratios determined by isotope dilution are low, <0·3, unlike typical residual mantle rocks, and are consistent with the LREE-enriched trace element patterns for clinopyroxene described above in which $(Nd)_n > (Sm)_n$. $^{87}Sr/^{86}Sr$ ratios vary between 0·7025 and 7·037, suggesting that the alteration products that resulted from the interaction between the crystals and seawater—which has a $^{87}Sr/^{86}Sr$ of 0·709—were almost completely removed from the samples by the careful sample preparation methods prior to digestion. This was also confirmed by the trace element analyses of the bulk separates, which yielded very low mobile element concentrations (Fig. 6a).

The $^{87}Sr/^{86}Sr$ and $^{143}Nd/^{144}Nd$ isotope ratios plot below or close to the mantle array (Fig. 7a). One clinopyroxene fraction (M3-1B) has a slightly higher $^{87}Sr/^{86}Sr$ than the other fractions, but another fraction of the same sample (M3-1A) plots on the mantle array, suggesting that M3-1B
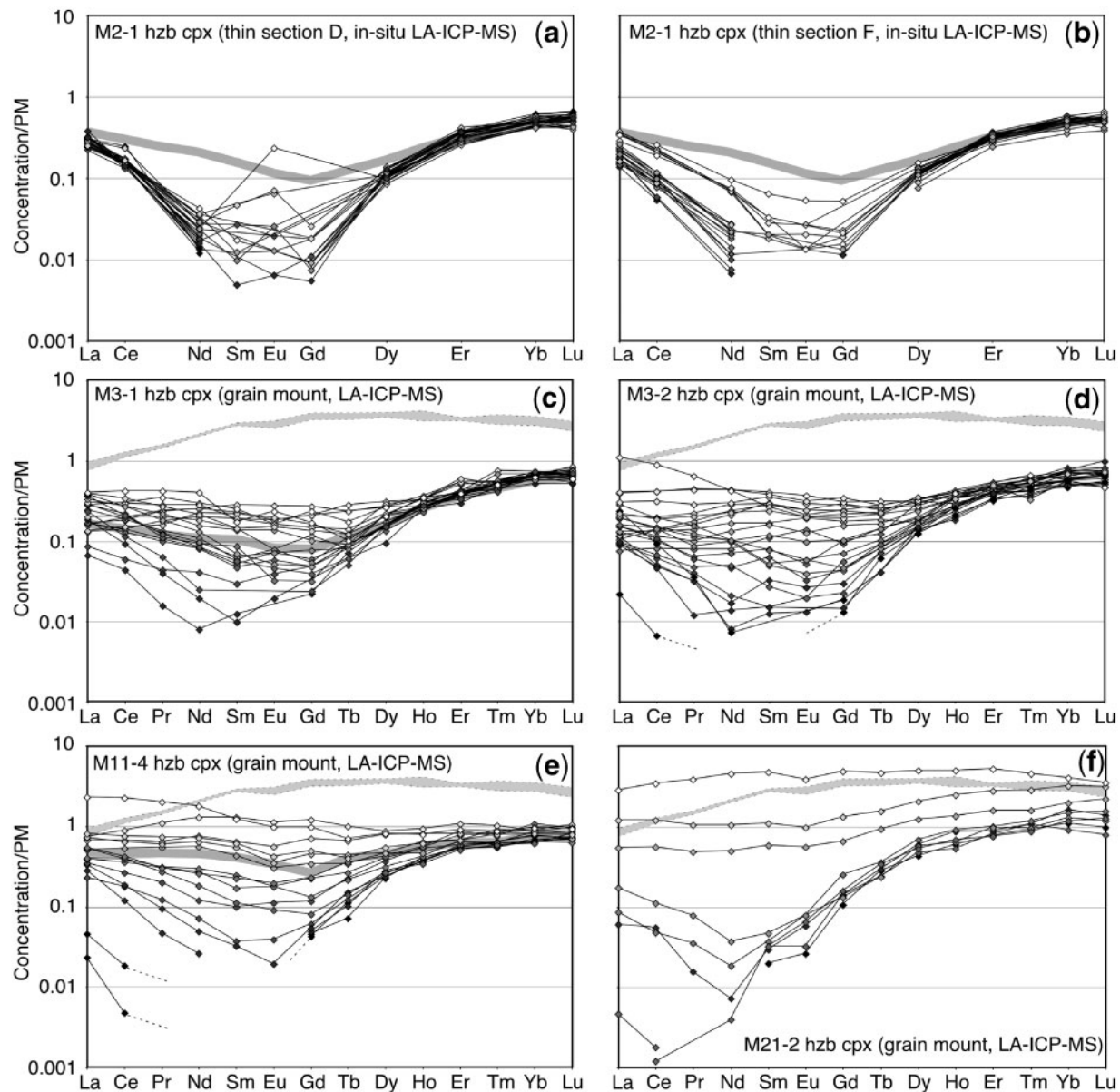
Fig. 5. Rare earth element patterns for clinopyroxene from Macquarie Island peridotites determined by LA-ICP-MS. (a, b) Data for two thick sections of sample M2-l, measured *in situ*. (c–f) Data for four samples measured on epoxy-mounted clinopyroxene mineral separates. Grey field indicates compositions of clinopyroxene from gabbroic veins Ml1-5 also measured by LA-ICP-MS. Dark grey line in (a)–(c) and (e) indicates the corresponding composition of the bulk analysis of 20–30 mg clinopyroxene batches. All concentrations are normalized to Primitive Mantle (McDonough & Sun, 1995).

contains some seawater alteration material that was not completely removed. The Macquarie Island samples plot at the lower end of the range of Nd and Sr isotope ratios in typical abyssal peridotites (Snow *et al.*, 1994; Salters *et al.*, 2002). More significantly, they overlap with values of the gabbroic vein and of the least enriched volcanic glasses found on Macquarie Island from the study of Kamenetsky *et al.* (2000), as shown in Fig. 7b.

HSE concentrations and Re–Os data for mantle rocks

Whole-rock samples of the macroscopically vein-free peridotite, as well as the gabbroic vein Ml1-5 from the Boot Hill area discussed above, were analyzed for HSE concentrations and Os isotopes. In the case of sample M2-l, we also analyzed a 2 g aliquot of a
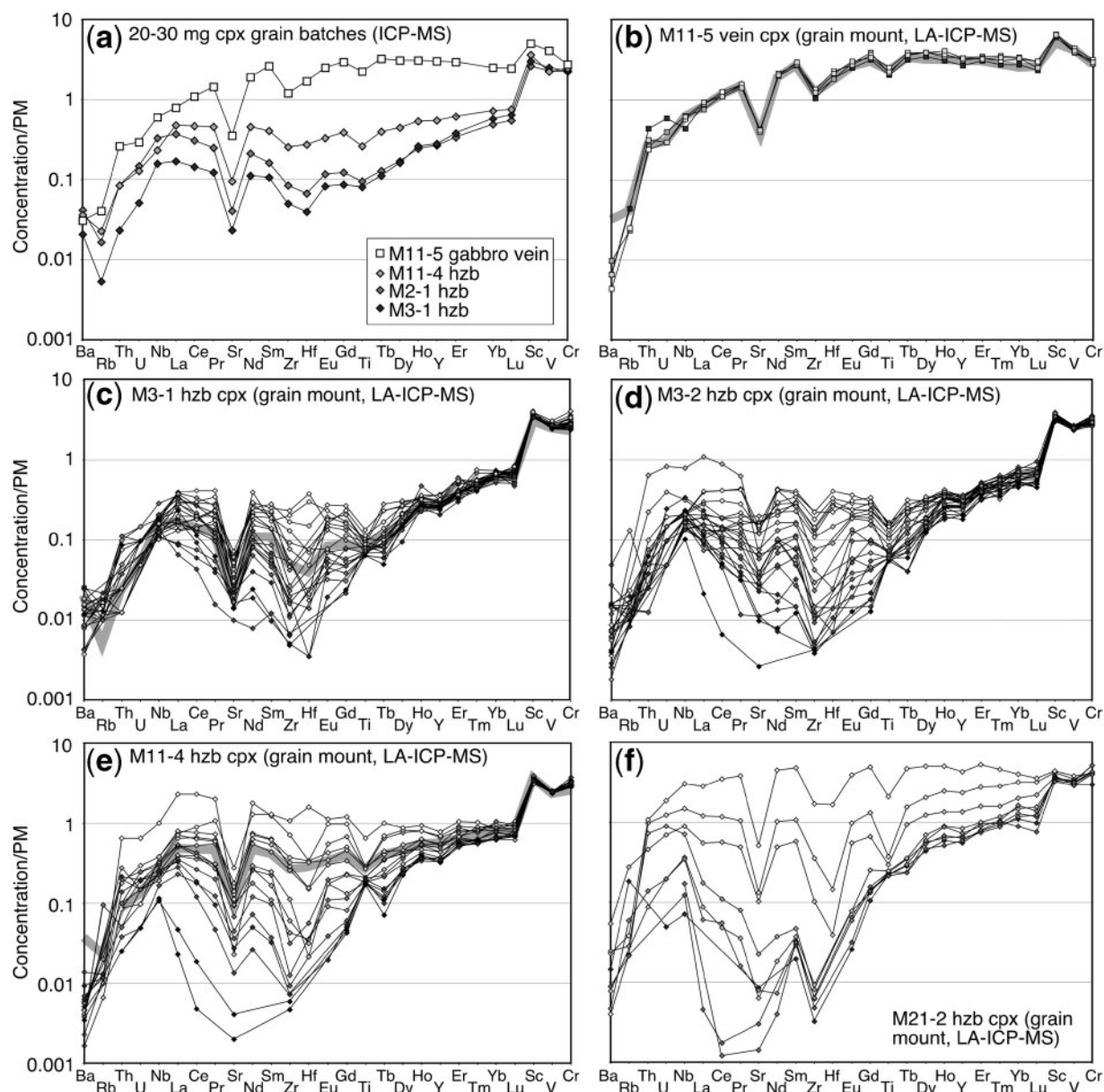
Fig. 6. Primitive mantle normalized trace element patterns for clinopyroxene from Macquarie Island peridotites and from the gabbroic vein. (a) Data determined for batches of separated clinopyroxene grains from four samples measured by solution ICP-MS. (b–f) Data for gabbroic vein and four peridotites on epoxy-mounted crystals, measured by LA-ICP-MS. Dark grey line in (b), (c) and (e) indicates the corresponding composition of the bulk analysis of 20–30 mg clinopyroxene batches. All concentrations normalized to Primitive Mantle (McDonough & Sun, 1995).

hand-picked, agate-milled, orthopyroxene mineral separate. Orthopyroxene was selected because SEM analysis showed rare small (<10 μm) Fe–Ni sulfide grains—generally expected to be important carriers for highly siderophile elements in mantle rocks—as inclusions, typically associated with clinopyroxene exsolution lamellae.

Data are presented in Table 5. The peridotite HSE patterns (Fig. 8) are flat or have a residual pattern characterized by a downward slope towards the most incompatible HSE (Pd and Re). In contrast, the gabbroic vein has a magmatic pattern with concentrations of Pt, Pd, and Re that exceed the concentrations of the more compatible Os, Ir, and Ru, but with altogether lower concentration levels than the peridotite

Table 4: Sm and Nd concentrations determined by isotope dilution and Sr and Nd isotope analyses on clinopyroxene separates from peridotites and from a gabbroic vein within the peridotites (M11-5)

Sample*	Sm (ppm)	Nd (ppm)	$^{147}Sm/^{144}Nd$	$^{143}Nd/^{144}Nd$	±2SE	$^{87}Sr/^{86}Sr$	±2SE
M2-1.A	0·047	0·206	0·1381	0·513063	0·000025	0·703215	0·000017
M2-1.B	0·067	0·291	0·1399	0·513066	0·000020	0·702859	0·000034
M3-1.A	0·034	0·129	0·1603	0·513127	0·000042	0·702964	0·000015
M3-1.B	0·034	0·128	0·1590	0·513073	0·000030	0·703725	0·000020
M3-2	0·041	0·145	0·1728	0·513045	0·000020	0·702915	0·000016
M3-2.R	0·042	0·145	0·1737	0·513139	0·000020	0·702789	0·000020
M11-4	0·159	0·548	0·1750	0·513082	0·000020	0·702563	0·000011
M11-4.R	0·168	0·566	0·1796	0·513063	0·000020	0·702619	0·000015
M21-2	0·856	2·319	0·2230	0·513067	0·000020	0·702744	0·000022
M11-5	0·976	2·173	0·2714	0·513067	0·000020	0·702463	0·000017

*A and B samples represent different batches of cpx from same sample with slightly different paramagnetic properties. R denotes replicate analyses.

samples. Some peridotite samples also show distinct Pt and Ru spikes, which can probably be attributed to the presence of small, distinct Pt- and Ru-rich minerals. Measured $^{187}Os/^{188}Os$ isotope ratios (0·1195–0·1229) are lower (less radiogenic) than typical present-day mantle rocks.

DISCUSSION
Late-stage melt percolation and melt–rock reactions

Some key features related to late-stage melt percolation are introduced here because the effects of these late-stage processes need to be addressed before the preceding melting history of the peridotites, in particular the degree of melting, can be assessed. The entire late-stage melt-percolation and subsolidus history of these peridotites will be the subject of a forthcoming paper.

The Macquarie Island peridotites provide abundant field, textural, major and trace element evidence for an important role of melt percolation and melt–rock reactions relatively late in their history. In the field, millimeter- to centimeter-scale gabbroic veins are widespread. In the Eagle Bay area, abundant meter-scale evolved gabbro bodies intrude the peridotites, and the peridotites grade upwards into plagioclase-dunites. These features suggest that melts traversed the peridotites in a localized way.

Textural evidence for pervasive porous melt flow and concomitant melt–rock reactions causing modal metasomatism can be found in all samples (Fig. 2). Textures are strikingly similar to those in peridotites from Ocean Drilling Program (ODP) Hole 1274A at the Fifteen–Twenty Fracture zone, discussed in detail by Suhr *et al.* (2008). Orthopyroxene clasts have a corroded, holly leaf-like or skeletal appearance, containing numerous embayments of olivine (Fig. 2a). Such textures are generally considered to be evidence for porous flow of orthopyroxene-undersaturated melts, which dissolve orthopyroxene by a melt-producing melt–rock reaction (e.g. Kelemen *et al.*, 1992; Dijkstra *et al.*, 2003; Piccardo *et al.*, 2006; Suhr *et al.*, 2008). A second type of texture is represented by the clinopyroxene selvages and clinopyroxene ± olivine ± spinel grains at the grain boundaries of orthopyroxene, often forming embayments (Fig. 2b and e). These textures probably represent reaction textures, where orthopyroxene is replaced by clinopyroxene, with or without olivine and spinel. This reaction consumed melt, as phases rich in Ca and Al, elements enriched within basaltic melt compared with mantle rocks, were produced at the expense of orthopyroxene. A fourth type of texture consists of intergrowths of spinel + clinopyroxene (Fig. 2c), resembling symplectites, that can be found at orthopyroxene grain boundaries or within the olivine matrix, another melt-consuming melt–rock reaction in which Ca- and Al-rich phases were newly formed (see Suhr *et al.*, 2008). Finally, there are small interstitial clinopyroxene crystals and trails of interstitial clinopyroxene crystals ('diffuse microveins', Fig. 2f) within the olivine matrix of the rocks, and 0·1–10 mm clinopyroxene ± plagioclase (micro-)veins (Fig. 2d). These are all interpreted as igneous crystallization or reaction products of percolating melts. For more detailed interpretations of almost identical textures, the reader is referred to the comprehensive paper by Suhr *et al.* (2008). The key issue is
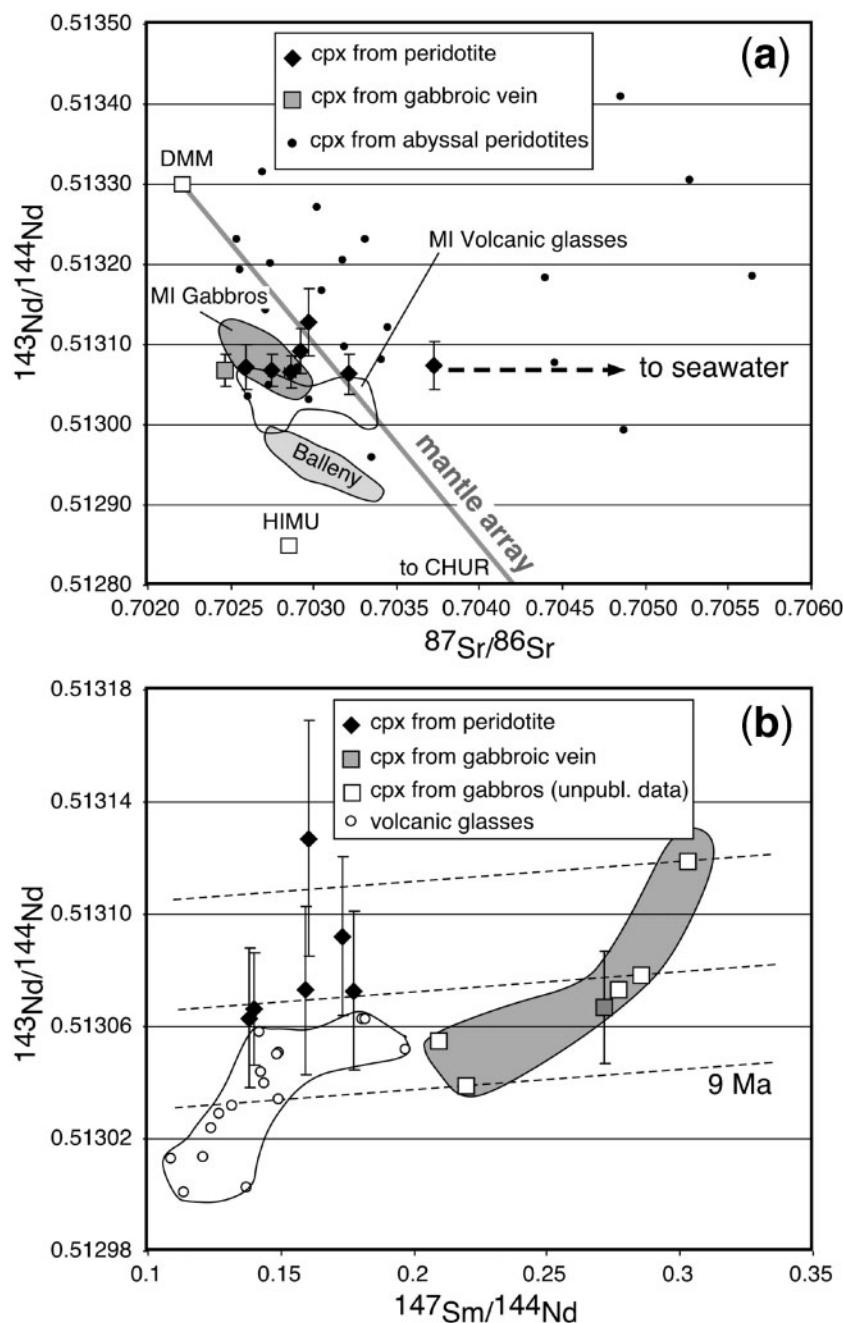
Fig. 7. Nd and Sr isotope data for peridotites on Macquarie Island. (a) $^{143}Nd/^{144}Nd$ vs $^{87}Sr/^{86}Sr$ for clinopyroxene and separates from peridotites and gabbroic vein; abyssal peridotite clinopyroxene data from Snow *et al.* (1994) and from Salters & Dick (2002) shown for comparison. (b) $^{143}Nd/^{144}Nd$ vs $^{147}Sm/^{144}Nd$ for the same samples. Error bars indicate 2σ errors. Thin dashed lines in (b) indicate 9 Ma isochrons, to allow comparison of samples with different Sm/Nd ratios. Also shown are data for volcanic glasses (Kamenetsky *et al.*, 2000; Kamenetsky & Maas, 2002), data for gabbroic rocks (A. H. Dijkstra, unpublished data), and data for nearby Balleny Islands OIB from Lanyon *et al.* (1995).

that all the clinopyroxene present in the Macquarie Island peridotites can be explained as exsolution from orthopyroxene, as products of melt-consuming melt–rock reaction features, or as crystallization products of a melt. The intricate shapes of the interstitial clinopyroxene and the

spinel–clinopyroxene intergrowths or symplectites suggest that these reactions occurred late in the geological history of the peridotites, post-dating any major deformation.

Despite the fact that we found few dunite layers in the field, none wider than 10 cm, the spinel grains preserve

Table 5: Highly siderophile element concentration data and Os isotope ratios for Macquarie Island samples

		[Os] (ng/g)	[Ir] (ng/g)	[Ru] (ng/g)	[Pt] (ng/g)	[Pd] (ng/g)	[Re] (ng/g)	$^{187}Re/^{188}Os$	$^{187}Os/^{188}Os$	±uncert.	$^{187}Os/^{188}Os$ (9 Ma)	t_{MA}* (Ga)	t_{RD}† (Ga)
Gabbro vein within peridotites													
M11-5	WR	0·151	0·118	0·21	0·94	0·76	0·24	7·6	0·1274	0·0026	0·1263	0·0	
M11-5.R	WR	0·153							0·1254	0·0021			
Harzburgites													
M2-1	WR	3·02	1·97	30·9	16·7	3·38	0·05	0·08	0·1206	0·0004	0·1206	1·32	1·06
M2-1o	opx	1·57	1·54	1·84	4·45	2·87	0·02	0·08	0·1227	0·0079	0·1227	0·94	0·76
M2-1o.R	opx	2·37							0·1220	0·0010	0·1220‡	1·06	0·85
M3-1	WR	4·93	2·65	3·98	8·69	11·5	0·03	0·03	0·1229	0·0013	0·1229	0·79	0·73
M3-2	WR	2·82	1·58	4·11	41·4	0·87	0·03	0·05	0·1195	0·0004	0·1194	1·42	1·23
M3-3	WR	1·89	0·68	5·24	6·02	1·25	0·52	1·3	0·1225	0·0015	0·1223	<0	0·78
M11-1	WR	4·56	3·45	4·82	7·52	1·32	0·06	0·06					
M11-3	WR	3·86	2·77	4·72	5·67	1·74	0·15	0·19	0·1227	0·0006	0·1226	1·45	0·76
Reference materials (means of repeat analyses)													
TDB-1 ($n=7$)		0·11	0·08	0·22	5·6	21·0	0·78						
OKUM ($n=8$)		1·1	1·1	4·7	15·1	11·6	0·58						
GAS ($n=1$)			3·0										

In sample numbers, R denotes replicate analysis of a different aliquot from same sample powder; WR, whole-rock; opx, clean orthopyroxene mineral separate.
*Model ages in Ga calculated assuming a present-day value for the bulk upper mantle of $^{187}Re/^{188}Os = 0·40186$ and $^{187}Os/^{188}Os = 0·1278$ and a decay constant of $1·67 \times 10^{-11}$/year.
†Re-depletion ages calculated in same way as model ages but assuming $[Re]_{sample} = 0$.
‡Assuming a Re/Os ratio identical to the two other analyses of this sample.
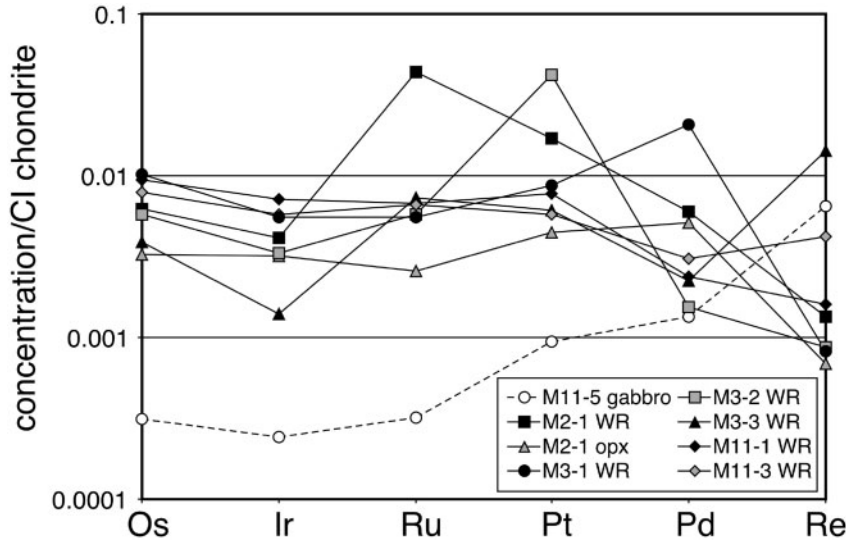

Fig. 8. Highly Siderophile Element (HSE) concentrations for Macquarie Island peridotites (whole-rocks) normalized to Cl chondrite (Anders & Grevesse, 1989), plotted with increasing incompatibility to the right.

chemical features that are typically associated with significant replacive dunite formation processes; that is, with dissolution of pyroxene and formation of olivine (Kelemen *et al.*, 1992, 1995; Suhr *et al.*, 2008). The trend of increasing TiO_2 concentration with increasing Cr-number in spinel is identical to that found within dunites and in dunite–harzburgite transition zone rocks from the Fifteen–Twenty Fracture Zone region (Suhr *et al.*, 2008; Fig. 3b). It is consistent with the widespread textural evidence for corrosion of orthopyroxene clasts by orthopyroxene-undersaturated melts, which, ultimately, produces dunite. It seems that, in the case of Macquarie Island, these reactions did not proceed to the point at which numerous, large-scale dunites were formed.

Probably the most important source of information about the melt-percolation history comes, in our case, from the measured clinopyroxene trace element patterns. As a result of our approach of analyzing separated clinopyroxene from a large sample volume, in combination with clinopyroxene crystals in thick sections, we obtain a more complete picture of the considerable within-rock variation in clinopyroxene trace element concentrations (Figs 5 and 6). Each sample is characterized by trace element patterns that show a strikingly large range of MREE concentrations, with much less variation in the LREE and the incompatible high field strength elements (HFSE; e.g. Th, U, Nb, Ta) and large ion lithophile elements (LILE; e.g. Ba, Rb), and very little variation in HREE and compatible elements such as Sc, V and Cr. Some clinopyroxene grains have deep MREE valleys, whereas others have almost flat REE patterns.

Evidence for cryptic metasomatism in the form of U-shaped to flat trace element patterns can best be explained by chromatographic processes associated with percolation of melt low-melt-fraction through peridotite. Percolation of hydrous melts can probably be ruled out, because of the low LILE concentrations and low Th/Nb ratios in clinopyroxene. During low-melt-fraction silicate melt percolation, the relative speed with which chemical fronts move through a column of rock are dependent on the compatibility of the element. The chemical fronts of the most incompatible elements move with almost the same velocity as the melt front, whereas the chemical fronts of the less incompatible elements (such as the HREE) move much more slowly, resulting in trace element fractionation within the percolating melt ('chromatographic effects', e.g. Navon & Stolper, 1987; Godard *et al.*, 1995; Vernières *et al.*, 1997). Percolation of basaltic liquid through a column of depleted peridotite with initial trace element patterns with LREE < MREE < HREE (i.e. the pattern after melt extraction) initially produces U-shaped trace element patterns in both rock and melt as the chemical fronts of LREE move through the rock and increase the LREE concentrations of the peridotites. The REE patterns become flat with continuing melt percolation when the chemical fronts of the MREE move through. This is a transient process and eventually, when also the chemical fronts of the more compatible HREE move through the rock, all the REE element concentrations are increased simultaneously until complete equilibrium between the rock column and the melt injected at the base of the column is achieved. The clinopyroxene trace element patterns in Figs 5 and 6 of samples M3-1 and M3-2 are consistent with melt percolation at low melt–rock ratio to the point at which the chemical fronts of the MREE passed through, whereas some clinopyroxene in samples M11-4 and M21-2 have also recorded transit of the chemical fronts of the HREE.

The observed within-rock variation in clinopyroxene trace element patterns is almost certainly related to the textural mode of occurrence. In sample M2-1, for which the clinopyroxene trace element data were obtained by *in situ* analysis of thick sections, the lowest MREE concentrations were found in clinopyroxene included within orthopyroxene, occurring on orthopyroxene grain boundaries, or forming part of clinopyroxene–spinel intergrowths, whereas the shallowest MREE valleys were found in clinopyroxene forming 'diffuse microveins' within the olivine matrix. Separated clinopyroxene with flat patterns and/or increased overall REE concentrations that trend towards the concentrations within the gabbroic veins therefore most probably originate from rare microveins or melt pockets. The negative Sr anomalies in clinopyroxene from the peridotites as well as from the gabbroic vein support the view that there is a close relation between the melt–rock reaction features in the peridotites and the abundant plagioclase-bearing magmatic veins and dykes that cross-cut the peridotites. For the Macquarie Island peridotites, melt percolation never led to crystallization of interstitial plagioclase in the peridotite matrix, but otherwise the harzburgites have many characteristics of plagioclase-peridotites.

As a first approximation, we assume that the percolating melt had the same composition as the melt that formed the centimeter-scale gabbroic vein of sample M11-5. If we compare the LILE concentrations of the clinopyroxene in the peridotites with those of the clinopyroxene in M11-5 we can see that the concentrations are almost identical, suggesting that melt–rock equilibrium for the LILE was reached during percolation. The concentrations of La in the peridotite clinopyroxene approach that of the vein clinopyroxene, and both peridotites M3-2 and M11-4 contain clinopyroxene in which the La concentrations even slightly exceed that of the vein clinopyroxene. This probably suggests that the percolating melt was indeed very similar to, or slightly more enriched in La than the melt that formed the gabbroic vein M11-5.

Three clinopyroxene grains separated from peridotite sample M21-2 strongly resemble clinopyroxene in the gabbroic vein in terms of their trace element composition; these clinopyroxene grains can either indicate re-equilibration as a result of chromatographic processes during melt percolation to the point at which complete equilibrium was attained, or they are 'magmatic'; that is, they crystallized from the percolating melt. The latter is likely, as we observed millimeter-scale clinopyroxene veins in thin sections of this sample, and it is possible that not all vein material was removed prior to crushing. Importantly, there is a complete trace element compositional continuum between clinopyroxene exsolved or formed by melt–rock reactions and 'true' magmatic clinopyroxene in veins. Despite the fact that a model involving only chromatographic processes can account for the observed shapes and trends of the trace elements patterns, the textural evidence suggests that clinopyroxene, and other phases, also crystallized during melt percolation. The implications of a coupled model that involves both chromatographic processes and modal changes (Vernières *et al.*, 1997) will be discussed in a subsequent paper on the melt percolation history of the Macquarie Island peridotites. The key conclusion of this paper, that the peridotites were highly depleted in trace elements prior to melt percolation, remains, independent of the details of the percolation model.

Implications of the melt percolation for Nd isotopes

A consequence of the extensive melt percolation is that most of the Nd within the batches of separated clinopyroxene used for Nd isotope analysis is derived from the percolating melt, as the Nd budget of the separates is dominated by clinopyroxene grains that have flat patterns with elevated (1–2 orders higher) concentrations of Nd compared with clinopyroxene grains with deep MREE valleys. Therefore, it is perhaps no surprise that the analyzed bulk Nd isotope compositions of the Macquarie Island peridotite samples are identical within error to those of the gabbroic vein, and to the crustal rocks on Macquarie Island in general (Fig. 7). Importantly, however, this confirms that the melt percolation was related to magmatic processes occurring at the Miocene ridge system where the overlying oceanic crust was formed. Moreover, the Nd isotope ratios of the peridotites do not overlap with those of the most enriched Macquarie Island volcanic glasses from the study of Kamenetsky *et al.* (2000). Instead, they are isotopically similar to the N-MORB-like volcanic glasses from this study. In the case of peridotite from ODP Hole 1274A at the Fifteen–Twenty Fracture Zone, is was argued that U-shaped trace element patterns identical to those found in our study were produced by interaction with strongly LREE-enriched liquids derived from pyroxenite melting (Seyler *et al.*, 2007). The

chromatographic model does not require such strongly LREE-enriched melts. Moreover, the isotopic composition of the Macquarie Island peridotites also shows that it is unlikely that such LREE-enriched mantle-heterogeneity-derived melt interacted to any significant extent with the studied mantle rocks, as they would certainly have left their imprint in the form of significantly lower $^{143}Nd/^{144}Nd$ isotope ratios [overlapping with E-MORB-like glasses of the study of Kamenetsky *et al.* (2000)] than observed.

Melting history and highly refractory character of the mantle

Petrological indicators for the degree of depletion in mantle peridotites suggest that the Macquarie Island harzburgites are unusually refractory. The key indicators for this highly refractory nature are: (1) low modal abundance of clinopyroxene; (2) high Cr-number in spinel; (3) low Al_2O_3 concentrations in the cores of orthopyroxene clasts; (4) low HREE concentrations and strongly fractionated HREE ratios in clinopyroxene.

The modal amount of clinopyroxene is very low, less than 2%, and we conclude on the basis of textures that all the clinopyroxene either was exsolved from orthopyroxene during subsolidus cooling or was produced by late-stage melt–rock reaction. In other words, there is no truly residual clinopyroxene left; hence, these rocks probably melted beyond the point of clinopyroxene disappearance from the residue (∼20–25% melt extraction, Hellebrand *et al.*, 2002; Barth *et al.*, 2003).

The Cr-number of spinel grains that are least modified by dunite-forming melt–rock reaction processes (i.e. the low-TiO_2 spinel) are 0·39–0·45, and are among the highest found so far in abyssal peridotites, indicating very high degrees of melt extraction (Dick & Bullen, 1984; Hellebrand *et al.*, 2001). They are comparable only with mantle spinel from the fast-spreading East Pacific Rise (Dick & Natland, 1996), and from the Fifteen–Twenty Fracture Zone at the slow-spreading Mid-Atlantic Ridge (Seyler *et al.*, 2007; Suhr *et al.*, 2008).

The major element compositions and core–rim variations of orthopyroxene clasts record subsolidus cooling of the peridotites. The coupled decrease of Al_2O_3 and Cr_2O_3 from core to rim in orthopyroxene (Fig. 4) is consistent with the reaction of Mg-Tschermak's component (in orthopyroxene) plus forsterite reacting to spinel and enstatite with decreasing temperature (Witt-Eickschen & Seck, 1991). However, by comparing the measured compositions of Macquarie Island orthopyroxene, in particular the core analyses, with compositional data from other oceanic peridotites, we can still extract qualitative constraints on the degree of melt extraction prior to subsolidus re-equilibration. Cores of orthopyroxene clasts have lower Al_2O_3 concentrations than orthopyroxene cores from
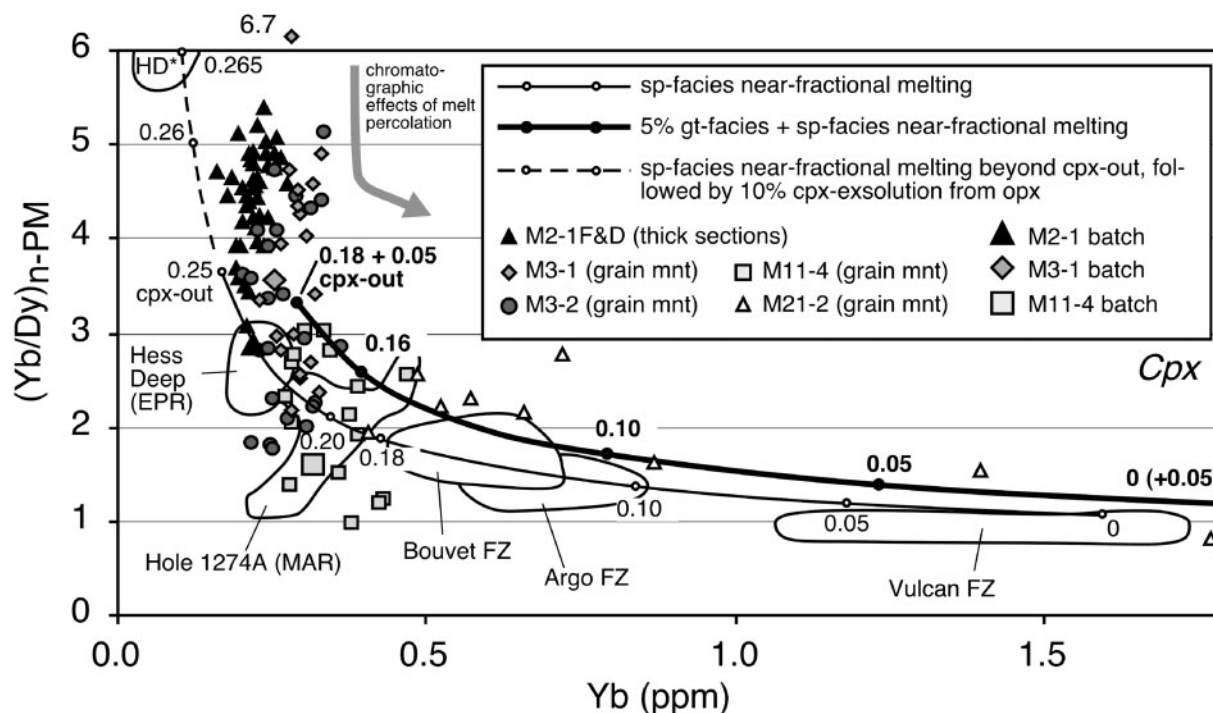
Fig. 9. Results of non-modal spinel-peridotite melting model. Model parameters are given in Table A4 (supplementary dataset). Near-fractional melting consists of iterative steps of 0·1% batch melting up to 25%. Dashed curve indicates melting beyond the point of cpx exhaustion, followed by transformation of 10% of existing orthopyroxene into clinopyroxene (by exsolution or melt–rock reaction; see discussion in text). Tick marks on curve with numbers indicate fraction of melt extracted. For comparison, a melting curve for 0–18% near-fractional melting in the spinel field after an initial 5% of near-fractional melting in the garnet field (after Hellebrand et al., 2002) is also shown. Such a model can explain compositions that are offset from the spinel-field-only melting curves to higher Yb/Dy ratios. Data sources for abyssal peridotite fields shown: Johnson et al. (1990), Dick & Natland (1996), Ross & Elthon (1997), Hellebrand et al. (2002), Seyler et al. (2007). HD* indicates composition of one outlier sample from Hess Deep.

anywhere along the Southwest Indian Ridge (SWIR, Seyler et al., 2003), and also lower than orthopyroxene from the 'extremely depleted peridotites' from south of the Kane Fracture Zone at the Mid-Atlantic ridge (MAR) in the study of Ross & Elthon (1997). Orthopyroxene is comparable only in terms of Al_2O_3 depletion with orthopyroxene in abyssal peridotites from the East Pacific Rise (EPR) [e.g. from Hess Deep (Dick & Natland, 1996) and from the Garrett and Terevaka Transform Faults (Niu & Hékinian, 1997)] or in peridotites from the Fifteen–Twenty Fracture Zone at the Mid-Atlantic Ridge (Seyler et al., 2007).

Clinopyroxene crystals least affected by melt–rock interaction (chromatographic processes and melt-impregnation) have low HREE concentrations and steep HREE slopes [e.g. $(Yb/Dy)_n$], as shown in Fig. 5. During melting and melt-extraction, the concentration of the more incompatible Dy in clinopyroxene should decrease faster than that of Yb, leading to an increase of $(Yb/Dy)_n$ and a decrease in Yb with progressive melt extraction. This is shown by the model curves for near-fractional melting in the spinel peridotite field, and for near-fractional

melting in the garnet-peridotite field followed by melting in the spinel-peridotite field in Fig. 9 (melting models based on Johnson et al., 1990; Johnson & Dick, 1992; Hellebrand et al., 2002; Barth et al., 2003; parameters used are given in Table A4, supplementary dataset). The Macquarie Island clinopyroxene has lower Yb and higher $(Yb/Dy)_n$ than typical, highly depleted abyssal peridotites, and is comparable only with clinopyroxene from Hess Deep (Dick & Natland, 1996), and from the Fifteen–Twenty Fracture Zone (Seyler et al., 2007; Suhr et al., 2008). However, there are two reasons why the Macquarie Island clinopyroxene compositions cannot be compared directly with the modeled clinopyroxene compositions in Fig. 9: first, clinopyroxene crystals are not simple source residua; second, they record late-stage melt percolation processes that affected their HREE concentrations, although to a much lesser extent than their LREE–MREE concentrations.

The effects of melt percolation need to be 'undone' before the degree of melting can be assessed quantitatively. Chromatographic effects during melt percolation would have increased the Dy concentration before the Yb

concentration, because of the higher incompatibility of Dy, decreasing the Yb/Dy slope as seen in Fig. 5. This would be followed by a coupled increase of both Dy and Yb with continuing melt percolation, after the chemical front for both elements passed through the rock. Therefore, points with the highest Dy/Yb ratios and the lowest Yb concentrations best reflect the compositions of the clinopyroxene before they were affected by melt percolation. These pre-melt percolation trace element concentrations are the most depleted compositions found so far in abyssal peridotites, except for one sample from Hess Deep (Dick & Natland, 1996), and cannot be explained as residues of near-fractional melting as they lie beyond the point of clinopyroxene exhaustion (Fig. 9).

The conclusion that the trace element composition suggests melting beyond the point of clinopyroxene exhaustion is consistent with the textural observations that neither the clinopyroxene in the Macquarie Island samples, nor that from the Fifteen–Twenty Fracture Zone, is truly residual. Most of the Macquarie Island clinopyroxene was exsolved from orthopyroxene during subsolidus cooling, or formed by melt–rock reactions at the expense of orthopyroxene (i.e. after melting). To estimate the degree of melting of the Macquarie Island peridotites we need to model the melting of orthopyroxene, and the trace element partitioning between ortho- and clinopyroxene during the subsequent clinopyroxene formation process. This is not straightforward, as mineral/melt partition coefficients for orthopyroxene, and for spinel, are less well known than for clinopyroxene. None the less, we investigated the effect by simply continuing our melting models with unchanged mineral/melt partition coefficients beyond the point of clinopyroxene exhaustion [at 25% melting in our model; compared with at 20–25% melting in the experiments of Baker & Stolper (1994)]. We tracked the bulk-rock and the orthopyroxene composition during further melting, keeping modal clinopyroxene at zero. At each step we also calculated what the clinopyroxene composition would be if 10% of the orthopyroxene present formed clinopyroxene (by exsolution or by melt–rock reaction), assuming closed-system behaviour and perfect trace element equilibrium between clinopyroxene and the other phases present. These clinopyroxene compositions are shown by the dashed curve in Fig. 9. The results show that melting beyond the point of clinopyroxene exhaustion depletes the rock so rapidly in trace elements that, to a first approximation, details of the model are irrelevant. In our model, only 1% of extra melting, followed by clinopyroxene formation, produces the extremely depleted compositions seen in the Macquarie Island samples. The amount of cpx-absent melting needed depends on the model parameters, but will always be extremely small. In essence, any small amount of melting beyond cpx-out will produce highly depleted compositions such as seen in the

Macquarie Island rocks. It should be noted that melt productivity in peridotite drops considerably after the disappearance of clinopyroxene from the residue (e.g. Baker & Stolper, 1994), so high degrees of cpx-absent melting are unlikely anyway under realistic mantle conditions.

Most analyses plot above and to the right of the spinel peridotite field melting curves; that is, the steepness of the HREE slope at a given HREE concentration cannot be perfectly explained by spinel field melting. Melting of peridotite in the presence of garnet, followed by melting in the spinel field produces steeper HREE slopes than spinel-field melting alone (Hellebrand *et al.*, 2002; Barth *et al.*, 2003), and such a model can explain the Macquarie Island data well. Figure 9 suggests that the peridotites may have undergone up to 5% melting in the garnet peridotite field, followed by melting in the spinel peridotite field to, and slightly beyond, clinopyroxene exhaustion.

The crust–mantle link

The unusual, enriched composition of the crustal section on Macquarie Island can be explained by the slow- to ultraslow spreading ridge setting in which these rocks were formed during the Miocene. In such settings the oceanic mantle lithosphere is thought to be thick, suppressing shallow-level mantle melting. The thick lithosphere implies that there was a significant contribution of melts derived from low-melting-point, high-melt-productivity, incompatible-element-enriched mantle heterogeneities (such as pyroxenites), which tend to melt out completely at the deeper levels of the melting column underneath a spreading centre (Michael *et al.*, 2003). At faster-spreading ridges with thinner lithospheric lids, such enriched melt fractions are mixed with larger amounts of more depleted melt fractions produced by shallow-level peridotite melting, resulting in less extreme, and, on average, more depleted magmas. Such a model requires that the overall degree of melting of the mantle source underneath the Macquarie ridge system was relatively low. The extremely depleted character of the peridotites rules out any genetic link of the exposed peridotites with the overlying crust on Macquarie Island; that is, the peridotites cannot represent the source residue of the oceanic crust. The last melts extracted from such highly refractory mantle were almost certainly depleted-MORB, or even high-SiO_2, boninite-like basalts, instead of the observed N- to ultra-E-MORB. Moreover, the high degrees of melt extraction are not compatible with the relatively thin crustal section on the island (<3 km on the northern part of the island, Dijkstra & Cawood, 2004), nor with the slow to ultraslow spreading rate of the Macquarie Island spreading centre in the Miocene. Finally, the refractory character of these peridotites, and thus, their high melting point, requires that the last melting occurred under either anomalously hot or wet

conditions, both of which seem unlikely for the Miocene seafloor-spreading event. The corroded orthopyroxene crystals suggest that some melt was produced by melt–rock reaction, but significant Miocene melting can probably be ruled out. Most probably, the highly refractory peridotites exposed on Macquarie Island record a previous melting event that is unrelated to Miocene seafloor spreading in the region. The Nd isotopes give no insight into the age of this melting event, as they were completely reset by late-stage melt percolation at the Miocene spreading center. Constraints on the age of this early melting event can, however, be obtained from the Os isotope data, as outlined in the following section.

Interpretation of the HSE and Re–Os isotope data

HSE concentration ratios in the Macquarie Island peridotite whole-rock samples confirm the refractory character of the rocks. Measured Os/Ir ratios of 1·5–2·8 significantly exceed the near-unity Os/Ir ratios (1·1 ± 0·2) for a large, global dataset of peridotites, mostly lherzolitic, in the study of Becker *et al.* (2006). The high Os/Ir ratios are similar to values for refractory harzburgite from the Troodos Ophiolite (1·2–2·9; Büchl *et al.*, 2002). These results confirm that Os is slightly more compatible than Ir in highly refractory peridotite (Becker *et al.*, 2006). One peridotite (M3-3) has an elevated Re concentration with respect to the other samples, leading to a relatively high Re/Os ratio of 0·274 compared with the other samples (0·01–0·044), but the high Re concentration is not associated with high Pt or Pd concentrations. The Re is almost certainly hosted in microscopic late-stage sulfides. The Re/Os ratios in the other samples are at the low end of the range of Re/Os ratios (0·00–0·48) in the peridotite dataset of Becker *et al.* (2006). This, together with the overall sparsity of sulfides, as well as the presence of distinct peaks in the PGE patterns, suggests that the PGEs are predominantly hosted in PGE alloys in the Macquarie Island samples (see Luguet *et al.*, 2007).

Given the low Re/Os ratios of the Macquarie Island peridotite, age corrections on the measured $^{187}Os/^{188}Os$ ratios back to 9 Ma are insignificant (of the order of 0·0001, 0·0002 in the case of M3-3; see Table 5) compared with the analytical error, and only uncorrected ratios for peridotites are discussed below. The $^{187}Os/^{188}Os$ values for the peridotites are highly non-radiogenic (0·1194–0·1229) with respect to estimates for present-day primitive upper mantle (PUM; 0·128–0·1296, Walker *et al.*, 2002; Meisel *et al.*, 1996, 2001). They are typically less radiogenic than the values for abyssal peridotite (0·1221–0·1270, mean of 0·125) from the study of Snow & Reisberg (1995), and correspond to the lower end of the large range of values (0·1183–0·1582) found in abyssal peridotite and Cr-spinel in the study of Standish *et al.* (2002). In contrast, the 9 Ma age-corrected $^{187}Os/^{188}Os$ ratio for the gabbroic vein

(0·1263) is significantly higher than that for the peridotite, and is well within estimates typical for PUM or abyssal peridotite. This confirms once more that the exposed peridotite is not the source residue of the melts that formed the gabbroic veins in the mantle. The veins, and probably the entire oceanic crust, must have been derived from a different, probably deeper mantle source.
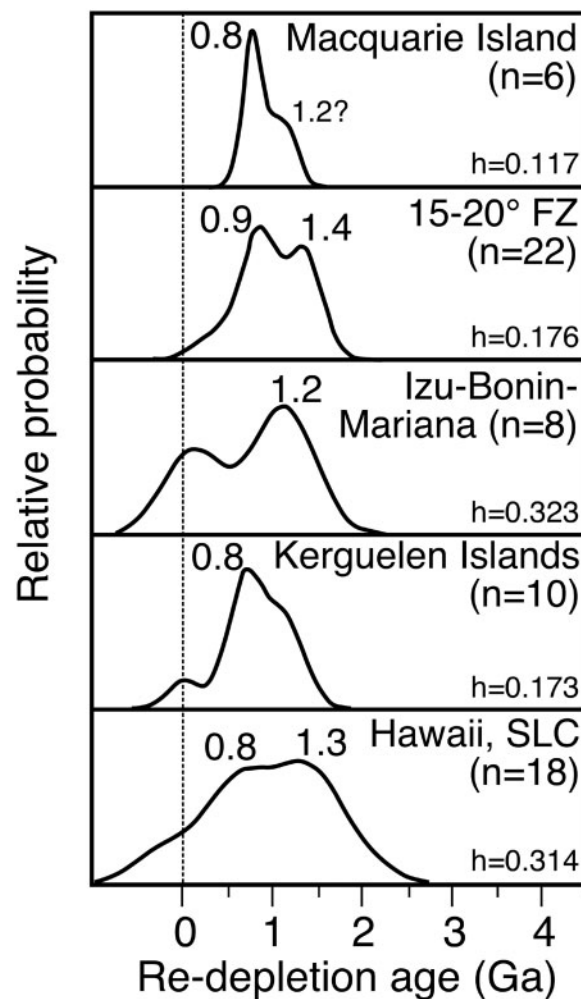

Fig. 10. Probability density diagrams (or kernel density estimations) of rhenium-depletion ages for key occurrences of highly refractory mantle rocks from young ocean basins and of xenoliths from ocean islands. All ages based on whole-rock Os isotope data. Re-depletion ages are based on reported Os isotope ratios and $^{187}Os/^{188}Os$ and $^{187}Re/^{188}Re$ ratios for PUM of 0·1278 and 0·40186 respectively, and assuming a present-day Re/Os ratio in the sample of zero. Probability density functions were calculated using the approach of Pearson *et al.* (2007), but with uncertainties ['bandwidths' h (Ga), value shown in lower right corner of each panel] based on Silverman's Rule of Thumb (see Rudge, 2008) assigned to each age. Data sources: Macquarie Island (this study); Fifteen–Twenty Fracture Zone (MAR) from Harvey *et al.* (2006); Izu–Bonin–Mariana fore-arc mantle from Parkinson *et al.* (1998); Kerguelen Island, Mont Trapeze mantle xenoliths from Hassler & Shimizu (1998); Hawaii, Salt Lake Crater mantle xenoliths from Bizimis *et al.* (2007).

The very non-radiogenic $^{187}Os/^{188}Os$ compositions compared with typical upper mantle rocks suggest that the peridotite was depleted in Re with respect to Os a long time ago. Re-depletion model ages are 0·7–1·2 Ga (Table 5, Fig. 10). These are calculated assuming that all Re was extracted from the rock by mantle melting, and they are therefore minimum ages for the melt extraction event. These ages depend on the choice of the $^{187}Os/^{188}Os$ isotopic ratio for the present-day bulk upper mantle reservoir (0·1278, Walker *et al.*, 2002). Using a value of 0·1290 (Meisel *et al.*, 1996) instead gives model ages that are *c.* 200 Myr older. The ages suggest that the samples were melted to high degrees in Proterozoic times, and were not subsequently homogenized with typical, more radiogenic upper mantle. If the Os isotopic signature is indeed hosted in Os-bearing alloys, as suggested for these highly refractory peridotites, it is easy to imagine how they could have avoided homogenization: Os alloys with tens of weight per cent Os, once formed during a high-degree mantle melting episode, are unlikely to re-equilibrate with typical mantle containing, on average, around 3 ppb Os. Alternatively, if the samples had undergone partial homogenization with typical convecting mantle, the main melting event would be even older. The data do not preclude that the peridotite produced some melt at 9 Ma. Such a recent melting event would have lowered the Re/Os ratio, but would not have had any effect yet on the $^{187}Os/^{188}Os$ ratio because of the low decay constant of the Re–Os isotope system. Moreover, as discussed above, the anomalous wet or hot melting conditions required for Macquarie Island peridotite are unlikely for the Miocene Macquarie paleo-ridge system. The opposite, recent Re gain as a result of sulfide crystallization associated with the observed melt percolation or with hydrothermal alteration cannot be ruled out, and is probably the cause of the elevated Re/Os ratio of sample M3-3 compared with the other samples. Therefore, calculated Re–Os model ages in Table 5, based on the measured Re/Os ratios, are probably overestimates of the age of melting. The Re-depletion ages therefore give the best constraint on the (minimum) age of melting; that is, prior to 0·7–1·2 Ga.

These results show that the Macquarie Island peridotites record an old, probably Proterozoic depletion event, without having undergone significant homogenization with typical, more radiogenic mantle subsequently. The peridotites, therefore, seem to be derived from a fragment of anciently depleted upper mantle cropping out on Macquarie Island.

The geodynamic significance of anciently depleted highly refractory mantle

Mantle xenoliths with unradiogenic Os isotope ratios from the Kerguelen Islands (Indian Ocean) with Proterozoic Re depletion ages have been interpreted as samples of a fragment of stranded subcontinental mantle underlying the Kerguelen Plateau, left behind after Gondwana rifting (Hassler & Shimizu, 1998). Highly refractory mantle rocks at the Newfoundland passive margin (Müntener & Manatschal, 2006) may have a similar origin as old continental mantle. Similarly, ultramafic lenses in the Swiss Alps with unradiogenic Os isotope ratios and Proterozoic model ages were interpreted by Meisel *et al.* (1996) as fragments of old subcontinental mantle lithosphere, as were peridotites from Zabargad Island (Red Sea) with Proterozoic Re-depletion ages (Snow & Schmidt, 1999).

In the case of the Macquarie Island peridotite samples, an origin as subcontinental mantle lithosphere cannot be excluded, but is unlikely, even though the distance to the westernmost edge of the continental Campbell Plateau is only 350 km. A well-defined seafloor morphology consisting of a spreading fabric, associated fracture zones, and seamounts can be recognized within the South Tasman Ocean basin, and spreading-related magnetic anomalies can be identified in even the oldest parts of the basin (Wood *et al.*, 1996; Lamarche *et al.*, 1997; Massell *et al.*, 2000). Moreover, volcanic rocks on Macquarie Island, even though they have unusually enriched compositions, were derived from shallow-level, spinel-peridotite facies, asthenospheric melting (Kamenetsky *et al.*, 2000), suggesting that the underlying mantle source is oceanic. This means that any surface layer of (stretched) continental mantle, if present, can only be very thin. Nevertheless, because we have no evidence for Miocene melting in the exposed peridotites, they cannot be unequivocally deemed 'oceanic'.

Crucially, anciently depleted, highly refractory peridotites, very similar to those from Macquarie Island described here, are increasingly being recognized in oceanic settings. They have recently been reported from the Fifteen–Twenty Fracture Zone at the Mid-Atlantic Ridge (Harvey *et al.*, 2006; Seyler *et al.*, 2007; Godard *et al.*, 2008), at the Gakkel Ridge (Liu *et al.*, 2008), and from the Izu–Bonin–Mariana fore-arc (Parkinson *et al.*, 1998). Os isotopic model ages from these localities are typically Proterozoic (Fig. 10). The samples from the Fifteen–Twenty Fracture Zone in particular are strikingly similar in degree of depletion and in Os isotope ratios to those from Macquarie Island. Clearly, an origin as subcontinental mantle lithosphere for the Fifteen–Twenty Fracture Zone peridotites is even less likely than for Macquarie Island. So, how can the occurrence of nearly identical peridotites—in both cases anomalous considering the spreading rate of the ridge at which they are found—at two sites *c.* 15 000 km apart, be explained? Is it possible that these unusual peridotites are derived from rare 'outcrops' of an anciently depleted upper mantle reservoir, more depleted than typical depleted MORB-source mantle, that has

global significance but that has so far been overlooked because it is too depleted to produce basalts?

In another recent study, Simon *et al.* (2008) reported that so-called 'ultra-refractory' peridotites are a major type of mantle xenolith in basalts from ocean islands worldwide. These highly refractory peridotite xenoliths typically lack primary clinopyroxene, have orthopyroxene Al_2O_3 concentrations of $1-3$ wt %, and spinel Cr-numbers >0.4 (Simon *et al.*, 2008) and are, therefore, in essence identical to the peridotites from Macquarie Island. In the case of most of these samples, their depletion is thought to predate the formation of oceanic crust in the area where they are found, although many show imprints of more recent melt–rock reaction processes that caused refertilization (Simon *et al.*, 2008). Moreover, they often have old (Proterozoic or Archean) Re–Os model ages or Re depletion ages (Bizimis *et al.*, 2007; Simon *et al.*, 2008). These results show that anciently depleted, highly refractory peridotites are far from uncommon, and that they should be considered as a distinct and global reservoir; however, the shape, scale, and distribution of highly refractory domains in the mantle remain largely unconstrained.

The question remains as to how these peridotites acquired their highly refractory character. Melting beyond the point of clinopyroxene exhaustion requires anomalously hot or wet melting conditions. Highly refractory peridotites could represent samples that have been melted under wet conditions in fore-arc settings and have subsequently survived largely unmodified for a billion of years or longer. Alternatively, Pearson *et al.* (2007) have suggested that there have been distinct, pulsed melting events in Earth history, which coincide with peak production rates of continental crust. These mantle melting events could have been associated with global mantle events such as slab avalanches or whole-mantle overturns (Stein & Hofmann, 1994; Condie, 1998, 2000; Davies, 2007), which could have been associated with anomalous (hot or wet) conditions in the upper mantle. Re-depletion ages for peridotite samples from Macquarie Island, the Fifteen–Twenty Fracture Zone and the Izu–Mariana fore-arc are very similar, and the same is true for the refractory Hawaii and Kerguelen mantle xenolith samples, as well as for the refractory samples from Zabargad Island (Fig. 10). Collectively, they seem to point to at least one, possibly two, unusually high-degree melting episodes in Proterozoic times.

Regardless of these speculations as to the nature of the depletion, it seems now well established that anciently depleted highly refractory peridotites are an important element of the upper mantle. They could represent a mantle reservoir, but one that is essentially sterile; that is, one that produces no basalt (Liu *et al.*, 2008; Simon *et al.*,

2008). The preservation of such domains suggests that convective stirring or diffusional homogenization of the mantle is incomplete on a 1 Gyr timescale, at least for osmium. This may be related to the fact that Os is hosted in PGE alloys in refractory mantle rocks (Luguet *et al.*, 2007), which do not re-equilibrate easily once formed. These domains have the potential to have preserved key information about the global history of the Earth's mantle.

CONCLUSIONS

(1) Peridotites exposed on Macquarie Island are highly refractory. They lack primary clinopyroxene, contain spinel with high Cr-number ($0.40-0.49$) and orthopyroxene with cores that are poor in Al_2O_3 ($2.7-3.0$ wt %); whole-rocks have high Os/Ir ($1.5-1.8$) and low Re/Os (typically <0.002). The Macquarie Island peridotites are among the most refractory peridotites reported so far from modern oceans; they are comparable only with samples from the fast-spreading East Pacific Rise and with atypical samples from the Mid-Atlantic Ridge found near the Fifteen–Twenty Fracture Zone.

(2) Late-stage melt–rock reactions and melt percolation have left an important textural and trace element imprint in the peridotites. However, the least-affected incompatible trace elements (e.g. HREE) still record an extreme depletion of the peridotites prior to melt percolation. The HREE concentrations and HREE slopes are consistent with melting beyond the point of clinopyroxene exhaustion (i.e. $>20-25\%$ near-fractional melting).

(3) The refractory character of the peridotites is inconsistent with the overall enriched character of the crustal section on the island, the relatively thin (<3 km) crust, and the slow spreading rate, which all point to low degrees of partial melting in the mantle source. The absence of a genetic crust–mantle link probably indicates that the exposed peridotites record a previous, pre-Miocene melting event. Melts derived from a deeper mantle source traversed this lid of highly refractory peridotites, interacted with them, and formed the overlying crustal section.

(4) The unradiogenic $^{187}Os/^{188}Os$ isotope ratios (as low as 0.1194), and the associated Proterozoic ($0.7-1.2$) Re-depletion minimum ages, suggest that the exposed peridotites represent a kilometer-sized domain of anciently depleted mantle rocks that was not homogenized with typical, more radiogenic mantle, during the last $\sim$1 Gyr.

(5) The similarity of the Macquarie Island peridotites to other highly refractory abyssal peridotites with old Re-depletion ages worldwide, and to common highly refractory mantle xenoliths from ocean island basalts, suggests that they define a common mantle reservoir of highly refractory, anciently depleted mantle that has global significance. Such a reservoir does not have the ability of produce basalts, but it may preserve clues about the melting history of the mantle as a whole.

ACKNOWLEDGEMENTS

SUPPLEMENTARY DATA

Supplementary tables for this paper are available at *Journal of Petrology* online.

REFERENCES

Anders, E. & Grevesse, N. (1989). Abundances of the elements: meteoric and solar. *Geochimica et Cosmochimica Acta* **53**, 197–214.

Baker, M. B. & Stolper, E. M. (1994). Determining the composition of high-pressure mantle melts using diamond aggregates. *Geochimica et Cosmochimica Acta* **58**(13), 2811–2827.

Barth, M., Mason, P. R., Davies, G. R., Dijkstra, A. H. & Drury, M. R. (2003). Geochemistry of the Othris Ophiolite, Greece: Evidence for refertilization? *Journal of Petrology* **44**, 1759–1785.

Bazylev, B. A. & Kamenetsky, V. S. (1998). Genesis of peridotites from the ophiolite complex of Macquarie Island, southwestern Pacific Ocean. *Petrology* **6**, 335–350.

Becker, H., Horan, M. F., Walker, R. J., Gao, S., Lorand, J.-P. & Rudnick, R. L. (2006). Highly siderophile element composition of the Earth's primitive upper mantle: Constraints from new data on peridotite massifs and xenoliths. *Geochimica et Cosmochimica Acta* **70**, 4528–4550.

Bédard, J. H. (1994). A procedure for calculating the equilibrium distribution of trace elements among minerals of cumulate rocks, and the concentration of trace elements in coexisting liquids. *Chemical Geology* **118**, 143–153.

Bizimis, M., Griselin, M., Lassiter, J. C., Salters, V. J. M. & Sen, G. (2007). Ancient recycled mantle lithosphere in the Hawaiian plume: Osmium–Hafnium isotopic evidence from peridotite mantle xenoliths. *Earth and Planetary Science Letters* **257**, 259–273.

Blundy, J. & Wood, B. (1994). Prediction of crystal–melt partition coefficients from elastic moduli. *Nature* **372**, 452–454.

Brunelli, D., Seyler, M., Cipriani, A., Ottolini, L. & Bonatti, E. (2006). Discontinuous melt extraction and weak refertilization of mantle peridotites at the Vema lithospheric section (Mid-Atlantic Ridge). *Journal of Petrology* **47**, 745–771.

Büchl, A., Brügmann, G., Batanova, V. G., Münker, C. & Hofmann, A. W. (2002). Melt percolation monitored by Os isotopes and HSE abundances: A case study from the mantle section of the Troodos Ophiolite. *Earth and Planetary Science Letters* **204**, 385–402.

Christodoulou, C. (1994). Mineralogy of the Macquarie Island plutonic suite. Fractionation processes at shallow level magma chambers and controls on basalt major element chemistry. *Ofioliti* **19**, 217–245.

Condie, K. C. (1998). Episodic continental growth and supercontinents: a mantle avalanche connection? *Earth and Planetary Science Letters* **163**, 97–108.

Condie, K. C. (2000). Episodic continental growth models: afterthoughts and extensions. *Tectonophysics* **322**, 153–162.

Davies, G. F. (2009). Episodic layering of the early mantle by the 'basalt barrier' mechanism. *Earth and Planetary Science Letters* (in press).

Dick, H. J. B. & Bullen, T. (1984). Chromian spinel as a petrogenetic indicator in abyssal and alpine-type peridotites and spatially associated lavas. *Contributions to Mineralogy and Petrology* **86**, 54–76.

Dick, H. B. & Natland, J. H. (1996). Late-stage melt evolution and transport in the shallow mantle beneath the East Pacific Rise. In: Mével, C., Gillis, K. M., Allan, J. F. & Meyer, P. S. (eds) *Proceedings of the Ocean Drilling Program, Scientific Results, 147.* College Station, TX: Ocean Drilling Program, pp. 103–134.

Dijkstra, A. H. & Cawood, P. A. (2004). Base-up growth of ocean crust by multiple phases of magmatism: Field evidence from Macquarie Island. *Journal of the Geological Society, London* **161**, 739–742.

Dijkstra, A. H., Drury, M. R. & Vissers, R. L. M. (2001). Structure and petrology of plagioclase-peridotites in the West Othris Mountains (Greece): Melt impregnation in mantle lithosphere. *Journal of Petrology* **42**, 5–24.

Dijkstra, A. H., Barth, M., Drury, M. R., Mason, P. R. D. & Vissers, R. L. M. (2003). Diffuse porous melt flow and melt–rock reaction in the mantle lithosphere at a slow-spreading ridge: A structural petrology and LA-ICP-MS study of the Othris Peridotite Massif (Greece). *Geochemistry, Geophysics, Geosystems* **4**(8), doi:10.1029/2001GC000278.

Eggins, S. M., Woodhead, J. D., Kinsley, L. P. J., Mortimer, G. E., Sylvester, P., McCulloch, M. T., Hergt, J. M. & Handler, M. R. (1997). A simple method for the precise determination of ≥40 trace elements in geological samples by ICPMS using enriched isotope internal standardisation. *Chemical Geology* **134**, 311–326.

Godard, M., Bodinier, J.-L. & Vasseur, G. (1995). Effects of mineralogical reactions on trace element redistributions in mantle

rocks during percolation processes: A chromatographic approach. *Earth and Planetary Science Letters* **133**, 449–461.

Godard, M., Lagabrielle, Y., Alard, O. & Harvey, J. (2008). Geochemistry of the highly depleted peridotites drilled at ODP Sites 1272 and 1274 (Fifteen–Twenty Fracture Zone, Mid-Atlantic Ridge): Implications for mantle dynamics beneath a slow spreading ridge. *Earth and Planetary Science Letters* **267**(3–4), 410–425.

Goscombe, B. D. & Everard, J. L. (1998). Macquarie Island 1:10 000 Geological Map Series, sheet 1 Hobart: Mineral Resources Tasmania.

Goscombe, B. D. & Everard, J. L. (2001). Tectonic evolution of Macquarie Island: Extensional structures and block rotations in oceanic crust. *Journal of Structural Geology* **23**, 639–673.

Griffin, B. J. & Varne, R. (1980). The Macquarie Island ophiolite complex: Mid-Tertiary oceanic lithosphere from a major ocean basin. *Chemical Geology* **30**, 258–308.

Harvey, J., Gannoun, A., Burton, K. W., Rogers, N. W., Alard, O. & Parkinson, I. J. (2006). Ancient melt extraction from the oceanic mantle revealed by Re–Os isotopes in abyssal peridotites from the Mid-Atlantic ridge. *Earth and Planetary Science Letters* **244**, 606–621.

Hassler, D. R. & Shimizu, N. (1998). Osmium isotopic evidence for ancient subcontinental lithospheric mantle beneath the Kerguelen Islands, Southern Indian Ocean. *Science* **280**, 418–421.

Hauri, E. H., Wagner, T. P. & T. L. Grove, T. L. (1994). Experimental and natural partitioning of Th, U, Pb and other trace elements between garnet, clinopyroxene and basaltic melts. *Chemical Geology* **117**, 149–166.

Hellebrand, E., Snow, J. E., Dick, H. J. B. & Hofmann, A. (2001). Coupled major and trace elements as indicators of the extent of melting in mid-ocean-ridge peridotites. *Nature* **410**, 677–681.

Hellebrand, E., Snow, J. E., Hoppe, P. & Hofmann, A. W. (2002). Garnet-field melting and late-stage refertilization in 'residual' abyssal peridotites from the Central Indian Ridge. *Journal of Petrology* **43**, 2305–2338.

Hofmann, A. W. (1997). Mantle geochemistry: the message from oceanic volcanism. *Nature* **385**, 219–229.

Jackson, S. E. (2008). LAMTRACE data reduction software for LA-ICP-MS. In: Sylvester, P. (ed.) *Laser Ablation ICP-MS in the Earth Sciences: Current Practices and Outstanding Issues. Mineralogical Association of Canada, Short Course Series* **40**, 305–307.

Johnson, K. & Dick, H. B. (1992). Open system melting and temporal and spatial variation of peridotites and basalt at the Atlantis II Fracture Zone. *Journal of Geophysical Research* **97**(B6), 9219–9241.

Johnson, K., Dick, H. B. & Shimizu, N. (1990). Melting in the upper mantle: An ion microprobe study of diopsides in abyssal peridotites. *Journal of Geophysical Research* **95**(B3), 2661–2678.

Johnston, A. D. & Schwab, B. E. (2004). Constraints on clinopyroxene/melt partitioning of REE, Rb, Sr, Ti, Cr, Zr, and Nb during mantle melting: First insights from direct peridotite melting experiments at 1·0 GPa. *Geochimica et Cosmochimica Acta* **68**, 4949–4962.

Kamenetsky, V. S. & Maas, R. (2002). Mantle-melt evolution (dynamic source) in the origin of a single MORB suite: a perspective from magnesian glasses of Macquarie Island. *Journal of Petrology* **48**, 1909–1922.

Kamenetsky, V. S., Everard, J. L., Crawford, A. J., Varne, R., Eggins, S. E. & Lanyon, R. (2000). Enriched end-member of primitive MORB melts: Petrology and geochemistry of glasses from Macquarie Island (SW Pacific). *Journal of Petrology* **41**, 411–430.

Kelemen, P. B., Dick, H. J. B. & Quick, J. E. (1992). Formation of harzburgite by pervasive melt–rock reaction in the upper mantle. *Nature* **358**, 635–641.

Kelemen, P. B., Shimizu, N. & Salters, V. J. M. (1995). Extraction of mid-ocean ridge basalt from the upwelling mantle by focused flow of melt in dunite channels. *Nature* **375**, 747–753.

Lamarche, G., Collot, J. Y., Wood, R. A., Sosson, M., Sutherland, R. & Delteil, J. (1997). The Oligocene–Miocene Pacific plate boundary, south of New Zealand: Evolution from oceanic spreading to strike-slip faulting. *Earth and Planetary Science Letters* **148**, 129–139.

Lanyon, R., Crawford, A. J. & Eggins, S. M. (1995). Westward migration of Pacific Ocean upper mantle into the Southern Ocean region between Australia and Antarctica. *Geology* **23**, 511–514.

Liu, C.-Z., Snow, J. E., Hellebrand, E., Brügmann, G., von der Handt, A., Büchl, A. & Hofmann, A. (2008). Ancient, highly heterogeneous mantle beneath Gakkel ridge, Arctic Ocean. *Nature* **452**, 311–316.

Luguet, A., Shirey, S. B., Lorand, J.-P., Horan, M. F. & Carlson, R. W. (2007). Residual platinum-group minerals from highly depleted harzburgites of the Lherz massif (France) and their role in HSE fractionation of the mantle. *Geochimica et Cosmochimica Acta* **71**, 3082–3097.

Maas, R., Kamenetsky, M. B., Sobolev, A. V., Kamenetsky, V. S. & Sobolev, N. V. (2005). Sr, Nd, and Pb isotopic evidence for a mantle origin of alkali chlorides and carbonates in the Udachnaya kimberlite, Siberia. *Geology* **33**(7), 549–552.

McDonough, W. F. & Sun, S.-S. (1995). The composition of the Earth. *Chemical Geology* **120**, 223–253.

Meibom, A., Sleep, N. H., Chamberlain, C. P., Coleman, R. G., Frei, R., Hren, M. T. & Woodens, J. L. (2002). Re–Os isotopic evidence for long-lived heterogeneity and equilibration processes in the Earth's upper mantle. *Nature* **419**, 705–708.

Meisel, T., Walker, R. J. & Morgan, J. W. (1996). The osmium isotopic composition of the Earth's primitive upper mantle. *Nature* **383**, 517–520.

Meisel, T., Walker, R. J., Irving, A. J. & Lorand, J.-P. (2001). Osmium isotopic composition of mantle xenoliths: a global perspective. *Geochimica et Cosmochimica Acta* **65**, 1311–1323.

Meisel, T., Fellner, N. & Moser, J. (2003). A simple procedure for the determination of platinum group elements and rhenium (Ru, Rh, Pd, Re, Os, Ir and Pt) using ID-ICP-Ms with an inexpensive on-line matrix separation in geological and environmental materials. *Journal of Analytical Atomic Spectrometry* **18**, 720–726.

Michael, P. J. *et al.* (2003). Magmatic and amagmatic seafloor generation at the ultra-slow Gakkel Ridge, Arctic Ocean. *Nature* **424**, 956–961.

Müntener, O. & Manatschal, G. (2006). High degrees of melt extraction recorded by spinel harzburgite of the Newfoundland margin: The role of inheritance and consequences for the evolution of the southern North Atlantic. *Earth and Planetary Science Letters* **252**, 437–452.

Natland, J. H. & Dick, H. J. B. (2002). Stratigraphy and composition of gabbros drilled in Ocean Drilling Program Hole 735B, Southwest Indian Ridge: A synthesis of geochemical data. In: Natland, J. H., Dick, H. J. B., Miller, D. J. & Von Herzen, R. P. (eds) *Proceedings of the Ocean Drilling Project, Scientific Results, 176*, pp. 1–69, [online].

Navon, O. & Stolper, E. (1987). Geochemical consequences of melt percolation: the upper mantle as a chromatographic column. *Journal of Geology* **95**, 285–307.

Niu, Y. & Hékinian, R. (1997). Spreading-rate dependence of the extent of mantle melting beneath ocean ridges. *Nature* **385**, 326–320.

Niu, Y., Collerson, K., Batiza, R., Wendt, J. I. & Regelous, M. (1999). Origin of enriched-type mid-ocean ridge basalts at ridges far from mantle plumes: The East Pacific Rise at 11°20′N. *Journal of Geophysical Research* **104**(B4), 7067–7087.

Parkinson, I. J., Hawkesworth, C. J. & Cohen, A. S. (1998). Ancient mantle in a modern arc: osmium isotopes in Izu–Bonin–Mariana forearc peridotites. *Science* **281**, 2011–2013.

Pearce, N. J. G., Perkins, W. T., Wesgate, J. A., Gorton, M. P., Jackson, S. E., Neal, C. R. & Chenery, S. P. (1997). A compilation of new and published major and trace element data for NIST SRM 610 and NIST SRM 612 glass reference materials. *Geostandards Newsletter* **21**, 115–144.

Pearson, D. G., Parman, S. W. & Nowell, G. M. (2007). A link between large mantle melting events and continent growth seen in osmium isotopes. *Nature* **449**, 202–205.

Pettke, T. (2008). Analytical protocols for element concentration and isotope ratio measurements in fluid inclusions by LA-(MC-)ICP-MS. In: Sylvester, P. (ed.) *Laser Ablation ICP-MS in the Earth Sciences: Current Practices and Outstanding Issues. Mineralogical Association of Canada, Short Course Series* **40**, 189–219.

Piccardo, G. B., Zanetti, A., Poggi, E., Spagnolo, G. & Müntener, O. (2006). Melt/peridotite interaction in the Southern Lanzo peridotites: Field, textural and geochemical evidence. *Lithos* **94**, 181–209.

Quilty, P. G., Crundwell, M. P. & Wise, S. W., Jr (2008). Microplankton provide 9 Ma age for sediment in the Macquarie Island ophiolite complex. *Australian Journal of Earth Sciences* **55**, 1119–1125.

Ross, K. & Elthon, D. (1997). Extreme incompatible trace-element depletion of diopside in residual mantle from south of the Kane Fracture Zone. In: Karson, J. A., Cannat, M., Miller, D. J. & Elthon, D. (eds) *Proceedings of the Ocean Drilling Program, Scientific Results, 153.* College Station, TX: Ocean Drilling Program, pp. 277–284.

Rudge, J. F. (2008). Finding peaks in geochemical distributions: A re-examination of the helium–continental crust correlation. *Earth and Planetary Science Letters* **274**, 179–188.

Salters, V. J. M. & Dick, H. J. B. (2002). Mineralogy of the mid-ocean-ridge basalt source from neodymium isotopic composition of abyssal peridotites. *Nature* **418**, 68–72.

Salters, V. J. M. & Stracke, H. J. B. (2004). Composition of the depleted mantle. *Geochemistry, Geophysics, Geosystems* doi:10.1029/2003GC000597.

Seyler, M., Cannat, M. & Mével, C. (2003). Evidence for major-element heterogeneity in the mantle source of abyssal peridotites from the Southwest Indian Ridge (52° to 68°E). *Geochemistry, Geophysics, Geosystems* doi:10.1029/2002GC000305.

Seyler, M., Lorand, J.-P., Dick, H. J. B. & Drouin, M. (2007). Pervasive melt percolation reactions in ultra-depleted refractory harzburgites at the Mid-Atlantic Ridge, 15°20′N: ODP Hole 1274A. *Contributions to Mineralogy and Petrology* **153**, 303–319.

Simon, N. S. C., Neumann, E.-R., Bonadiman, C., Coltorti, M., Delpech, G., Grégoire, M. & Widom, E. (2008). Ultra-refractory domains in the oceanic mantle lithosphere sampled as mantle xenoliths at ocean islands. *Journal of Petrology* **49**(6), 1223–1251.

Snow, J. E. & Reisberg, L. (1995). Os isotopic systematics of the MORB mantle: results from altered abyssal peridotites. *Earth and Planetary Science Letters* **133**, 411–421.

Snow, J. E. & Schmidt, G. (1999). Proterozoic melting in the northern peridotite massif, Zabargad Island: Os isotopic evidence. *Terra Nova* **11**(1), 45–50.

Snow, J. E., Hart, S. R. & Dick, H. J. B. (1994). Nd and Sr isotope evidence linking mid-ocean ridge basalts and abyssal peridotites. *Nature* **371**, 57–60.

Standish, J. J., Hart, S. R., Blusztajn, J., Dick, H. J. B. & Lee, K. L. (2002). Abyssal peridotites osmium isotopic compositions from Cr-spinel. *Geochemistry, Geophysics, Geosystems* **9**(1), doi:10.1029/2001GC000161.

Stein, M. & Hofmann, A. W. (1994). Mantle plumes and episodic crustal growth. *Nature* **372**, 63–68.

Suhr, G., Kelemen, P. & Paulick, H. (2008). Microstructures in Hole 1274A peridotites, ODP Leg 209, Mid-Atlantic Ridge: Tracking the fate of melts percolating in peridotites as the lithosphere is intercepted. *Geochemistry, Geophysics, Geosystems* **9**(3), doi:10.1029/2007GC001726.

Sun, S.-S. & McDonough, W. F. (1989). Chemical and isotopic systematics of oceanic basalts: implications for mantle composition and processes. In: Saunders, A. D. & Norry, M. J. (eds) *Magmatism in the Ocean Basins. Geological Society, London, Special Publications* **42**, 313–345.

Sutherland, R. (1995). The Australian–Pacific boundary and Cenozoic plate motions in the SW Pacific: Some constraints from Geosat data. *Tectonics* **14**, 819–831.

Varne, R. & Rubenach, M. J. (1972). Geology of Macquarie Island and its relationship to oceanic crust. In: Hayes, D. E. (ed.) *Antarctic Oceanography II: The Australian–New Zealand Sector. American Geophysical Union, Antarctic Research Series* **19**, 251–266.

Varne, R., Brown, A. V. & Falloon, T. (2000). Macquarie Island: Its geology, structural history, and timing and tectonic setting of its N-MORB to E-MORB magmatism. In: Dilek, Y., Moores, E. M. & Nicolas, A. (eds) *Ophiolites and Oceanic Crust: New Insights from Field Studies and the Ocean Drilling Program. Geological Society of America, Special Papers* **349**, 301–320.

Vernières, L., Godard, M. & Bodinier, J.-L. (1997). A plate model for the simulation of trace element fractionation during partial melting and magma transport in the Earth's upper mantle. *Journal of Geophysical Research* **102**(B11), 24771–24784.

Waight, T. E., Baker, J. & Peate, D. (2002). Sr isotope ratio measurements by double-focusing MC-ICPMS: techniques, observations and pitfalls. *International Journal of Mass Spectrometry* **221**, 1–16.

Walker, R. J., Prichard, H. M., Ishiwatari, A. & Pimentel, M. (2002). The osmium isotopic composition of convecting upper mantle deduced from ophiolite chromitites. *Geochimica et Cosmochimica Acta* **66**, 329–345.

Wertz, K. L. (2003). From seafloor spreading to uplift: the structural and geochemical evolution of Macquarie Island on the Australian–Pacific plate boundary. PhD dissertation, University of Texas at Austin, 169 p.

White, W. M. & Schilling, J.-G. (1978). The nature and origin of geochemical variation in Mid-Atlantic Ridge basalts from the central North Atlantic. *Geochimica et Cosmochimica Acta* **42**, 1501–1516.

Witt-Eickschen, G. & Seck, H. A. (1991). Solubility of Ca and Al in orthopyroxene from spinel peridotites: an improved version of an empirical geothermometer. *Contributions to Mineralogy and Petrology* **106**, 431–439.

Wood, B. J. & Blundy, J. D. (1997). A predictive model for rare earth element partitioning between clinopyroxene and anhydrous silicate melt. *Contributions to Mineralogy and Petrology* **129**, 166–181.